Aspects of gorgonopsian paleobiology and evolution: insights from the basicranium, occiput, osseous labyrinth, vasculature, and neuroanatomy

Ricardo Araújo [Corresp., 1, 2, 3, 4, 5] , **Vincent Fernandez** [6] , **Michael J Polcyn** [7] , **Jörg Fröbisch** [2, 8] , **Rui M.S. Martins** [9, 10, 11]

[1] Instituto Superior Técnico, Universidade de Lisboa, Instituto de Plasmas e Fusão Nuclear, Lisboa, Portugal

[2] Museum für Naturkunde - Leibniz-Institut für Evolutions- und Biodiversitätsforschung, Berlin, Germany

[3] Southern Methodist Univesity, Huffington Department of Earth Sciences, Dallas, Texas, United States of America

[4] GEAL - Museu da Lourinhã, Lourinhã, Portugal, Germany

[5] Université de Montpellier 2, Institut des Sciences de l'Evolution, Montpellier, France

[6] European Synchrotron Research Facility, Grenoble, France

[7] Huffington Department of Earth Sciences, Southern Methodist University, Dallas, Texas, United States of America

[8] Institut für Biologie, Humboldt Universität Berlin, Berlin, Germany

[9] Instituto de Plasmas e Fusão Nuclear, Universidade de Lisboa, Lisboa, Portugal

[10] CENIMAT/I3N, Universidade Nova de Lisboa, Monte de Caparica, Portugal

[11] GEAL - Museu da Lourinhã, Lourinhã, Portugal

Corresponding Author: Ricardo Araújo
Email address: ricardo.araujo@tecnico.ulisboa.pt

Synapsida, the clade including therapsids and thus also mammals, is one of the two major branches of amniotes. Organismal design, with modularity as a concept, offers insights into the evolution of therapsids, a group that experienced profound anatomical transformations throughout the past 270Ma, eventually leading to the evolution of the mammalian bauplan. However, the anatomy of some therapsid groups remains obscure. Gorgonopsian braincase anatomy is poorly known and many anatomical aspects of the brain, cranial nerves, vasculature, and osseous labyrinth, remain unclear. We analyzed two gorgonopsian specimens, GPIT/RE/7124 and GPIT/RE/7119, using propagation phase contrast synchrotron micro-computed tomography. The lack of fusion between many basicranial and occipital bones in GPIT/RE/7124, which is an immature specimen, allowed us to reconstruct its anatomy and ontogenetic sequence, in comparison with the mature GPIT/RE/7119, in great detail. We explored the braincase and rendered various skull cavities. Notably, we found that there is a separate ossification between what was previously referred to as the "parasphenoid" and the basioccipital. We reinterpreted this element as a posterior ossification of the basisphenoid: the basipostsphenoid. Moreover, we show that the previously called "parasphenoid" is in fact the co-ossification of the dermal parasphenoid and the endochondral basipresphenoid. In line with previous descriptions, the anatomy of the osseous labyrinth is rendered in detail, revealing a unique

discoid morphology of the horizontal semicircular canal, rather than toroidal, probably due to architectural constraints of the ossification of the opisthotic and supraoccipital. In addition, the orientation of the horizontal semicircular canal suggests that gorgonopsians had an anteriorly tilted alert head posture. The morphology of the brain endocast is in accordance with the more reptilian endocast shape of other non-mammaliaform neotherapsids.

ASPECTS OF GORGONOPSIAN PALEOBIOLOGY AND EVOLUTION: INSIGHTS FROM THE BASICRANIUM, OCCIPUT, OSSEOUS LABYRINTH, VASCULATURE, AND NEUROANATOMY

ARAÚJO R.[1,2,3,4,5*], FERNANDEZ V.[6], POLCYN M.J.[3], FRÖBISCH J.[2,7], and MARTINS R.M.S.,[1,4,8]

[1]Instituto de Plasmas e Fusão Nuclear, Instituto Superior Técnico, Universidade de Lisboa, Lisboa, Portugal; [2]Museum für Naturkunde - Leibniz-Institut für Evolutions- und Biodiversitätsforschung, Berlin, Germany; [3]Huffington Department of Earth Sciences, Southern Methodist Univesity, Texas, United States of America; [4]GEAL - Museu da Lourinhã, Lourinhã, Portugal; [5]Institut des Sciences de l'Evolution, Université de Montpellier 2, Montpellier, France [6]European Synchrotron Radiation Facility, Grenoble, France; [7]Institut für Biologie, Humboldt-Universität zu Berlin, Berlin, Germany; [8]CENIMAT/I3N, Faculdade de Ciências e Tecnologia, Universidade Nova de Lisboa, Caparica, Portugal.

* Corresponding author

ABSTRACT

Synapsida, the clade including therapsids and thus also mammals, is one of the two major branches of amniotes. Organismal design, with modularity as a concept, offers insights into the evolution of therapsids, a group that experienced profound anatomical transformations throughout the past 270Ma, eventually leading to the evolution of the mammalian bauplan. However, the anatomy of some therapsid groups remains obscure. Gorgonopsian braincase anatomy is poorly known and many anatomical aspects of the brain, cranial nerves, vasculature, and osseous labyrinth, remain unclear. We analyzed two gorgonopsian specimens, GPIT/RE/7124 and GPIT/RE/7119, using propagation phase contrast synchrotron micro-computed tomography. The lack of fusion between many basicranial and occipital bones in the immature specimen GPIT/RE/7124 allowed us to reconstruct its anatomy and

ontogenetic sequence in comparison with the mature GPIT/RE/7119. We examined the braincase and rendered various skull cavities. Notably, there is a separate ossification between what was previously referred to as the "parasphenoid" and the basioccipital. We reinterpreted this element as a posterior ossification of the basisphenoid: the basipostsphenoid. Moreover, the "parasphenoid" is a co-ossification of the dermal parasphenoid and the endochondral basipresphenoid. Our detailed examination of the osseous labyrinth reveals a unique discoid, rather than toroidal, morphology of the horizontal semicircular canal that probably results from architectural constraints of the opisthotic and supraoccipital ossifications. In addition, the orientation of the horizontal semicircular canal suggests that gorgonopsians had an anteriorly tilted alert head posture. The morphology of the brain endocast is in accordance with the more reptilian endocast shape of other non-mammaliaform neotherapsids.

INTRODUCTION

Radical transformations in the synapsid skull arrangement led to the unique mammalian cranial design, however, the inner skull anatomy of some therapsid groups such as the gorgonopsians remains mostly unknown. Moreover, although many sensory systems leave fossil evidence in the braincase, the gorgonopsian braincase remains an obscure element of the pre-mammalian evolutionary record. This scarcity in detailed descriptions of the gorgonopsian braincase can be partly attributed to technological constraints. Indeed, while it is believed that gorgonopsians have a high degree of cranial homomorphism (Sigogneau-Russell 1989, Kammerer 2016), our knowledge of the braincase is largely based on external morphology and on destructive serial grinding. Several braincase elements are rarely exposed (e.g., prootic, epipterygoid; Kammerer, 2016) and even in the acid-prepared skulls described by Kemp (1969) the descriptions are terse. The ventral surface of the palate is the only basicranial aspect that has been thoroughly studied (Sigogneau-Russell 1989, Kammerer 2014). However, many features related to the neuroanatomy and sensory systems are on the dorsal surface of the basicranium and anterior surface of

the occiput. Olson (1938), Kemp (1969) and Sigogneau (1970) count among the few studies that provided significant insights into the basicranium and occiput. Nevertheless, many uncertainties remain as these braincase reconstructions mostly resulted from analyses of serial sectioning or specimens broken along a single plan. The gorgonopsian braincase is complex, particularly in older individuals where extensive co-ossification and fusion has taken place, thus making rendering interpretations rather challenging.

In recent years, non-destructive imaging of rare and fragile fossil specimens has greatly benefited paleontological studies by uncovering previously inaccessible anatomy. Here, we provide a detailed description of the gorgonopsian braincase by using propagation phase-contrast synchrotron radiation-based micro-computed tomography. We selected two specimens for analysis: GPIT/RE/7124 and GPIT/RE/7119. GPIT/RE/7124, previously attributed to *Aloposaurus gracilis*, was selected because it shows several osteologically immature features including a clear separation of the basicranial elements, which are typically co-ossified in osteologically mature specimens such as GPIT/RE/7119. The braincase of GPIT/RE/7124 has never been described in detail, with the exception of the posterior view of the occiput and the ventral view of the palate (von Huene 1937), and a more recent re-analysis of the specimen (Sigogneau-Russell 1989). GPIT/RE/7119 is a Tanzanian specimen that was initially described as *Dixeya nasuta* by von Huene (1950), and later reclassified as *Arctognathus*? *nasuta* by Sigogneau-Russell (1989). Gebauer (2007) maintained the ascription to this genus, however, Kammerer (2015) points several differences in GPIT/RE/7119 relative to the holotype of *Arctognathus*. Thus, the taxonomic content of the genus needs to be revised. We segmented all the individual bones of the occiput and braincase of GPIT/RE/7124 and GPIT/RE/7119 where it was possible to separate them. For GPIT/RE/7119, we also segmented the voids bounded by the basicranial bones (i.e., brain endocast, osseous labyrinth, cranial nerves and vasculature). Our results offer the first detailed insights into the gorgonopsian braincase.

Institutional Acronyms

BPI – Evolutionary Studies Institute (formerly Bernard Price Institute) University of Witwatersrand, Johannesburg, South Africa

GPIT - Institut und Museum für Geologie und Paläontologie, Eberhard Karls Universität, Tübingen, Germany

AMNH – American Museum of Natural History, New York, USA

RC – Rubidge Collection, Wellwood, South Africa

NHMUK – Natural History Museum, London, United Kingdom

UMZC – University Museum of Zoology, Cambridge, United Kingdom

Materials and Methods

Materials

GPIT/RE/7124 (Figure 1) was collected at Heuning Nest Krantz (also spelled: Heuningneskrans or Honingnest Krantz) in the district Graaff Reinet, South Africa (von Huene 1937), from strata considered to belong to the *Cistecephalus* Assemblage Zone (Kitching 1977, van der Walt et al. 2010), Wuchiapingian in age (Cohen et al. 2013), and from about 255-256 Ma (Rubidge et al. 2013). Von Huene (1937) ascribed this specimen to *Aloposaurus gracilis.* Unfortunately, information on the collector or the exact stratigraphic level is not provided in the original description of the specimen (von Huene 1937). Von Huene did not collect the specimen himself, but was able to obtain it from South Africa. It was prepared further possibly in Tübingen. The braincase is not explicitly described, there is a detailed description about the posterior view of the occiput and the ventral view of the palate (von Huene 1937), and later Gebauer (2007) redescribed the external anatomy of the specimen. Sigogneau (1970) reconsidered von Huene's systematic placement and allocated the specimen to Gorgonopsia incertae

sedis and later to *Aelurosaurus* (Sigogneau-Russell 1989). Thereafter, Gebauer (2007) recently revised the specimen and ascribed it to *Aelurosaurus wilmanae* on the basis of the following characters: a relatively broad snout, prefrontal large but short anteriorly, broad intertemporal space, transverse apophyses without teeth, occiput less inclined than in the other species.

GPIT/RE/7119 was found from a layer more than 40 m above the lower boundary of the Tanzanian equivalent of the *Cistecephalus* zone (Angielczyk et al. 2014) near the Kingori Mountain (von Huene 1950). Von Huene (1950) describes the anatomy and relationships of the specimen attributing it to the species *Dixeya nasuta*, later revised by Sigogneau (1970) and Gebauer (2007) as *Arctognathus*? *nasuta*, however this taxonomic placement is currently under revision (Kammerer 2015).

Propagation Phase Contrast Synchrotron micro-Computed Tomography

Both skulls GPIT/RE/7124 and GPIT/RE/7119 were scanned at the ID17 beamline of the European Synchrotron Radiation Facility (ESRF, Grenoble, France; proposal HG-23) using Propagation Phase Contrast Synchrotron Radiation-based micro-Computed Tomography. The setup consisted of a FReLoN-2k camera, a 0.3x magnification set of lenses, a scintillating fiber optic, a monochromatic X-ray beam of 100 keV and 150 keV respectively (bent double-Laue crystals) and a sample-detector distance of 10.9 m to perform Propagation Phase Contrast Synchrotron micro Computed Tomography (PPC-SRµCT). Tomographies were computed based on 4998 projections of 0.1 s for GPIT/RE/7124 and 0.2 s for GPIT/RE/7119, over 360 degrees resulting in data with an isotropic voxel size of 46.57 µm and 45.71 µm respectively. Additionally, the center of rotation was shifted to the size of the image (~45 mm and ~85 mm respectively) to increase the horizontal field of view in the reconstructed data (i.e., half acquisition protocol).

The tomographic reconstruction was performed using the single distance phase retrieval approach of the software PyHST2 (Paganin et al 2002, Mirone et al 2014). The ð/ß value was set to 1000

based on trial reconstructions (range tested 500-2000) as it was offering the best contrast for segmentation while not blurring the images. The resulting 32 bits data were converted to a stack of 16 bits tiff using 0.2 % saturation min and max values from the 3D histogram generated by PyHST2.

For GPIT/RE/7124, we performed two additional steps: first as the fossil contains large dense minerals (most likely metallic), it was not possible to adjust the contrast properly to differentiate bones from matrix without causing problematic saturation of the image. To limit this issue, we applied a high-pass filter on the dense structures, segmented using a threshold, using a 2D median with a window size of 3 pixels, preserving only edges of the dense material while decreasing their mean grey values. Secondly, as the flat field correction was not able to completely correct the vertical intensity gradient of the synchrotron beam, we applied a second 2D median filter with a window size of 250 pixels to normalize the mean grey values of each slice.

Segmentation of GPIT/RE/ 7124 was performed first on Amira 5.3 (FEI Visualization Sciences Group, Mérignac, France) on a 2x2x2 binned version of the volume to facilitate handling of the data set. We performed manual segmentation with masking and we mostly used tools like “brush” and “magic wand”. Measurements were taken using the 3D measurement tool in the actual segmentation. Secondly, the created surfaces were imported into the original, non-binned volume using VGStudio MAX 3.0 (Volume Graphics, Heidelberg, Germany). Region of interest (ROI) of bones were refined using region growing tool, bounded to the previous segmentation made on the binning version. Concerning the endocast, the ROI was dilated in 3D by 9 voxels, then smoothed with a strength of 50 pixels to ensure it would overlap surrounding bones when present and remove linear pattern from manual segmentation. We then removed the overlapping part by subtracting surrounding bone ROIs to the endocast ROI. To clearly identify parts of the endocast bounded by bones, we merged the ROIs of all bones into a single one, dilated it by 3 voxels and created a new ROI from its intersection with the endocast ROI. Then, on

the final rendering of the endocast, by showing the full endocast and intersection at the same time, part truly defined by surrounding bones are clearly shown, as well as part resulting from interpolation.

Before rendering we performed a 3D median filter with a window size of 3 voxels to decrease the noise at the surface of the bones. Finally we used volume rendering with the Phong algorithm, an oversampling of 5 and a density of 2 to generate images.

Virtual cross sections of GPIT/RE/7124 were generated on VGStudio MAX 3.0, using the thick slab mode, showing the average of 3 slices to decrease overall noise on the images.

ANATOMICAL DESCRIPTION OF THE BRAINCASE

Despite some plastic deformation previously described by Sigogneau (1970), the braincase and occiput region of GPIT/RE/7124 is moderately well preserved (Figure 2, 3, 4). GPIT/RE/7124 is somewhat dorsoventrally compressed, there is minor displacement of posterior occipital elements, and there are several fractures in the skull roof and occiput. Numerous metallic inclusions pervade through the specimen, but due to their small dimensions they did not affect segmentation. Due to fusion and fracturing, the sutures between the interparietal and tabulars were the most difficult to discern, therefore the actual morphology of these bones is here assumed to be tentative. Relevant structures, particularly those with ontogenetic importance, of the GPIT/RE/7119 are examined on the discussion, thus the following description is solely focused on the more complete and GPIT/RE/7124 braincase. The terms basipresphenoid and basipostsphenoid derive from the developmental literature, where they are regarded as subdivisions of the basisphenoid (Couly 1993).

Prootic

The right and left prootic are exquisitely preserved, providing new anatomical information. Only the anterior part of the right pila antotica (but see Kemp's 1969 opinion on the origin of this structure) did

not preserve and the left anterodorsal process (of Kemp 1969, *taenia marginalis* of Sigogneau-Russell 1989) is incompletely preserved in the left prootic.

The basal region contacts the parasphenoid-basipresphenoid anteriorly, the basipostsphenoid ventrally, the supraoccipital posterodorsally, the opisthotic posteroventrally, and the contralateral prootic medially. Although the anterior portion of the basioccipital extends far anteriorly, it does not contact the prootic (Figure 2 and 3). In the sellar region, posterior to the excavation on the basipresphenoid for the sella turcica, the prootic is conspicuously excavated laterally, forming the prootic embayment.

The parasphenoid-prootic suture runs over the anterior prootic buttress and posterior parasphenoid buttress. The suture with the parasphenoid is complex (Figure 5), the tubera flush with the lateral wall of the prootic and laterally, the two bones contact on an oblique suture superficially. However, the prootic sockets into the parasphenoid more deeply in a “stepped tongue in groove joint” (Jones et al. 2011).

There is a clear separation between the basipostsphenoid and prootic of about 260µm, contra Laurin (1998, p. 769). The two bones only contact in a few points anteriorly, but there is a clear sutural mark on the basipostsphenoid leaving a sub-rhomboid impression on the basipostsphenoid.

The prootic abuts the supraoccipital dorsally, becoming a broader contact ventrally where both bones are excavated to house the floccular fossa (sensu Sigogneau-Russell 1989, fig. 71, but named subarcuate fossa according to Olson 1937, 1938).

The prootic contacts via an interdigitating suture on the medial extension on the dorsal surface of the opisthotic (Figure 4A), becoming looser posteriorly. A fused opisthotic and prootic has been described for *Arctognathus* (Kammerer 2015, p. 48) and may be an ontogenetic feature.

The prootic has a dorsal supraoccipital-prootic notch, sloping to the anterodorsal process of the prootic. Between the anterodorsal process and the pila antotica there is an irregularly shaped notch, the

prootic fenestra of Kemp (1969). A shallow depression covers most of the prootic lateral surface, extending to the basal region. The anterior prootic notch is a deep excavation located on the anterior surface of the prootic, medial to the contact surface of the parasphenoid-basipresphenoid and ventral to the pila antotica. The two prootics contact each other medially, within the medullary cavity, and the contact is subtriangular in sagittal cross-section. The dorsal surface of the medial prootic process forms the dorsum sella of Kemp (1969; see also Sigogneau-Russell 1989). This is probably the same as the so-called basicranial process of the periotic of Olson (1944).

In posterior view, on the basal region of the prootic, there is a subtriangular fossa formed by the posterior crest of the medial prootic process, by the medial wall of the prootic and bordered ventrally by the dorsal surface of the basipostsphenoid (this study). A mediolaterally-oriented foramen, the facial foramen, pierces the lateral wall near the basal region of the prootic and exits at the base of the medial prootic process. This foramen has ~600µm diameter laterally and ~400µm at its mid-section.

There is no shallow depression posteroventral to the base of the anterodorsal process on the right prootic (contra Laurin 1998); however, on the left prootic there is indeed a shallow depression. Due to the asymmetry of this feature, differences may be the result of taphonomic distortion.

Basioccipital

The basioccipital forms the ventral border of the foramen magnum. The basioccipital contacts the exoccipital dorsolaterally, the opisthotic laterally and the basipostsphenoid anteriorly (Figure 2 and 3. The parasphenoid-basipresphenoid does not contact the basioccipital (contra Laurin 1998, fig.5; Parrington 1955, fig. 6 and 10). The articulation facet with the exoccipital is ellipsoidal in shape and dipping posteriorly. A clear separation between basioccipital and basipostsphenoid is discernible dorsally, but the two bones become co-ossified ventrally (Figure 6). The separation between the opisthotic is conspicuous (distance between the bones is 200-300µm), forming a ball-and-socket joint

(Figure 4 and 6). The articulation facet with the opisthotic is ellipsoidal, with the major axis dipping anteriorly.

The occipital condyle is reniform in shape, possessing a shallow median depression on its dorsal surface (Figure 7C). In ventral view, the occipital condyle is somewhat V-shaped (Figure 7 A). The articulation with the exoccipital is formed by a short dorsal process, which has an oblique orientation relative to this bone (Figure 7 B and F). The dorsal process slopes anteriorly into a shallow crest that meet its counterpart on the anterior tip of the basioccipital. The anterior part of the basioccipital forms a short, triangular-pyramidal process (Figure 7 A, E, F). The dorsal process of the basioccipital is pierced by the hypoglossal foramen (Figure 7 B and D), which served for the passage of the hypoglossal nerve (cn XII). The hypoglossal foramen is a horizontally-oriented canal with 600-800µm in diameter. The basioccipital forms the posteriormost part of the basal tubera, which continues onto the basipostsphenoid and parasphenoid. An ellipsoidal foramen perforates the ventral surface of the contact between the basioccipital and basipostsphenoid.

Exoccipital

The exoccipital has the typical subtriangular shape in posterior view described by Kemp (1969). It forms part of the lateral wall of the foramen magnum and contacts the basioccipital ventrally along its medial edge (Figure 2 A). The basioccipital is partially co-ossified to the exoccipital ventrally, but there is a clear separation dorsally between the two bones on the tomographs. The exoccipital does not contact the opisthotic. The exoccipital contacts the supraoccipital along its dorsal edge. The dorsal edge is sinusoidal on the right exoccipital but almost straight on the left. The posterior surface and the ventral margin of the exoccipital together with the ventromedial corner of the supraoccipital constitute the dorsal border of the jugular foramen (Figure 2 A). The exoccipital does not form part of the occipital condyle (contra Kemp 1969, p. 18).Kemp (1969, p. 19) describes a “small pyramidal exoccipital process”. This process is

probably best described as the pyramidal exoccipital crest that results from the ventral facet with the basioccipital and dorsal facet with the supraoccipital (Figure 8).

The exoccipital forms part of the anterior and dorsal wall for the passage of the glossopharyngeal and the vagoaccessory nerves (cn IX, X, XI), see also Colbert (1948). The exoccipital prevents the supraoccipital from contacting the basioccipital, although that element extends far ventrally.

Opisthotic

The opisthotic is a rod-like bone that contacts the supraoccipital dorsally, the basioccipital medially, the tabular on its posterolateral extremity, the squamosal on its anterolateral extremity and the prootic anteriorly (Figure 2 and 9). The ventral margin of the opisthotic is strongly concave, compared with its gently embayed dorsal margin. The opisthotic forms the ventral margin of the post-temporal fenestra and it contributes to the ventral margin of the jugular foramen on its anterodorsal extremity (Figure 2). The opisthotic and supraoccipital are firmly co-ossified, leaving no sutural marks (Figure 4 E).

The anterior surface of the opisthotic is dominated by an anteriorly-directed process that progressively thickens medially, serving as the posterior and lateral support of the prootic (Figure 9).

The lateral surface of the opisthotic is subcircular, and its gently convex lateral margin is carved by a lateral incisure (Figure 9 B, E). In cross-section, the opisthotic is subovoid at its median section, and subrectangular medially.

Supraoccipital

The supraoccipital is a rather complex element, however only its posterior occipital exposure is typically described (Figure 10). The supraoccipital is a single median element (Figure 4 B). The subrectangular

posterior exposure of the supraoccipital is only a small portion of the bone which extends significantly further dorsally but is covered by the tabular and interparietal in posterior view (Figure 2).

The supraoccipital is comprised of an alar region as well as the supraoccipital body (Figure 10). The supraoccipital body is a complex stout ventral structure that sutures with the prootics anteriorly, with the opisthotics ventrolaterally, and the exoccipitals posteriorly at its most ventromedial part (Figure 2). The alar region is wedged along its dorsal extension between the tabulars anteriorly and the squamosals posteriorly (Figure 10).

The supraoccipital body is a subrectangular buttress extending mediolaterally that encompasses: the anterior process (Kemp 1969, fig. 22B), the floccular fossa, the foramen for the posterior semicircular canal and the horizontal semicircular canal, and constitutes the articular facet for the prootic, opisthotic and exoccipital (Figure 10).

The anterior process projects dorsally from the medial surface of the supraoccipital body, forming the ventral margin of the floccular fossa and the base for the prootic suture (Figure 10 C, D). The prootic sutural facet is T-shaped rotated medially, with the base of the “T” being the anterior process. The suture with the opisthotic is a laterally-rotated U-shape, forming a deep fossa between the posterior surface of the opisthotic and the anterior surface of the supraoccipital (Figure 10 E, J).

The supraoccipital forms the dorsal border of the foramen magnum, forming the ventral supraoccipital embayment (Figure 2). An emargination on the ventrolateral edge of the supraoccipital alar region forms the dorsal margin of the posttemporal fenestra (Figure 2).

Basipostsphenoid

The basipostsphenoid is undeformed and completely preserved. It is composed of the basisphenoidal tubera on the ventral side and the subhexagonal main body (Figure 11). The anterior and posterior margins of the basipostsphenoid main body are concave.

A sheath of bone projecting posteriorly from the parasphenoid covers nearly half of the ventral surface of the basipostsphenoid (Figure 11). On each side of the dorsal surface of the basipostsphenoid there is a parabolic shaped crest that develops from the lateral corner towards its median section and inflects posteriorly towards the posterior corner of the basipostsphenoid (Figure 11 A).

Parasphenoid-basipresphenoid

The parasphenoid-basipresphenoid is pristinely preserved and it is only slightly plastically distorted as a result of mediolateral shear. The parasphenoid-basipresphenoid contacts the pterygoid along the parasphenoid rostrum anteriorly. Along its posterior border, the parasphenoid-basipresphenoid contacts the basipostsphenoid on the ventral half, and the prootic on the dorsal half. The interdigitating suture between the parasphenoid-basipresphenoid and basipostsphenoid is difficult to extricate, however, the separation between the prootic and parasphenoid-basipresphenoid is evident in the tomographs (Figure 6).

The parasphenoidal tubera are the most prominent feature in the ventral view of the parasphenoid (Figure 3, 12 C, G). The parasphenoidal tubera connect to the parasphenoid rostrum anteriorly via the anterior parasphenoidal lamina (Figure 12 G), and to the basisphenoidal tubera via the posterior parasphenoidal lamina (Figure 3, 12 G). The parasphenoidal tubera are somewhat triangular in shape and are significantly larger than the basisphenoidal tubera (Figure 11, 12). The posterior parasphenoid fossa (Figure 12) is a deep excavation delimited medially by the prootic and basipostsphenoid suture and by a crest that converges to the parasphenoidal tubera laterally. There is no basipterygoid process (contra Olson 1944, fig. 20).

The parasphenoid rostrum is deepest at the intersection of the right and left anterior parasphenoidal lamina (Figure 12 C). In lateral aspect, the ventral edge is slightly concave whereas the dorsal edge is convex, giving the rostrum a subtriangular shape. Two thin crests on the dorsal edge of

the parasphenoid rostrum form a trough (the vidian canal) on its posterior portion that meet at midlength (Figure 12 A, C).

On its dorsal side, the sella turcica is delimited laterally by the two saddle-shaped dorsal buttresses of the parasphenoid-basipresphenoid (the processus clinoideus?), and by the anterior prootic buttress as well as the medial prootic process posteriorly (contra Sigogneau-Russell 1989, who described the sella turcica as part of the basisphenoid). The sella turcica is divided in two ellipsoidal depressions separated by a short ridge (as in Olson 1944, Sigogneau-Russell 1989). The sella turcica is deeper posteriorly and becomes shallower anteriorly as the parasphenoid dorsal buttress slopes ventrally (Figure 12 A, H).

A horizontal trough, the vidian canal, separates the posterior parasphenoid buttress from the parasphenoid keel (Figure 12 E). On the posterior portion of the parasphenoid-basipresphenoid a medioanteriorly-directed foramen (~600µm) pierces the lateral surface of the parasphenoid-basipresphenoid at the level of the horizontal trough, the cerebral branch of the internal carotid (Figure 12 E). This foramen is L-shaped and exits the dorsal surface of the parasphenoid-basipresphenoid on a deep fossa anterior to the sella turcica, the hypophyseal fossa plus the exit for the cerebral branch of the internal carotids (Figure 12 A). Located anterior to the hypophyseal fossa, there are posteriorly-convex dome-shaped structures, separated by a median anteriorly-directed process that has been undescribed before, possibly a remnant of the orbitosphenoid (Figure 12 D).

Orbitosphenoid

Although the orbitosphenoid is nearly complete, it is lacking part of the lateral wall posteriorly and there is a dorsoventral crack traversing its anterior portion (Figure 13). Olson (1944 p.76) described the orbitosphenoid as laying in the dorsal groove of the parasphenoid, but although it is not as well preserved in this region it does not reach the parasphenoid.

335 The orbitosphenoid is a semi-cylindrical bone articulating with the frontal and parietal dorsally
336 and continues as a lateral wall ventrally from the sagittal axis of the skull (Figure 13 B). At the
337 intersection between the semi-cylindrical and lateral wall regions of the orbitosphenoid, two parallel
338 internal cavities extend along the posterior section of the bone (Figure 13 A).
339 The ventral region of the tubular region is smooth posteriorly, however, a median ridge raises at
340 about midlength of the frontal (Figure 13 A). The median ridge becomes progressively taller and more
341 acute, eventually forming a distinct separation between the two lobes of the olfactory bulb (Figure 13
342 D). On its anteriormost zone, the median ridge forms a distinct dorsally-inflated process that articulates
343 with the sagittal suture of the frontals.
344
345 **Tabular**
346 The tabular is subtriangular in shape with a raised lateral edge for articulation with the squamosal
347 (Figure 2, 14). The left tabular is well preserved, but the dorsal section of the right tabular is missing
348 (Figure 14). The tabular contacts the interparietal along its dorsal surface (Figure 14). The left tabular is
349 firmly sutured to the wing of the interparietal and it is very difficult to separate them on the basis of the
350 tomographs. In this case the external surface allows a better interpretation of the sutures. Most of the
351 anterior surface of the tabular makes the articular facet for the supraoccipital (Figure 14 B). The two
352 tabulars are separated in the sagittal plane of the skull by the interparietal (Figure 14).
353
354 **Interparietal**
355 The interparietal is incompletely preserved with the right wing being significantly incomplete. There is a
356 break between the more robust median section of the interparietal, comprising the nuchal crest, and
357 the left wing (Figure 14). The nuchal crest bulges slightly more dorsal than the ventral border of the
358 interparietal and tapers dorsally. There is a small foramen that traverses mediolaterally the interparietal

wing away from the nuchal crest (Figure 4 I). The suture between the interparietal and the tabular is hard to discern using the tomographs.

Squamosal

Only the dorsal ramus of the squamosal is preserved in both sides, thus missing the zygomatic portion (Figure 2, 15 A). The preserved squamosal contacts the tabular posteriorly and the supraoccipital medially. The articular surface for the tabular extends dorsoventrally along a vertical crest delimiting its lateral border and flares anteriorly into an elongated subtriangular process (Figure 15). Part of the squamosal sulcus is preserved in posterior view forming a flat area posteriorly (Figure 15 A). The supraoccipital articular facet forms an embayment on the surface of the squamosal delimited by a parabolic crest (Figure 15 A, D). The quadrate recess of the squamosal is a deeply excavated depression delimited posteriorly and dorsally by a subcircular crest (Figure 15 B).

Brain endocast

Three sections of the skull offer reliable proxies of the brain endocast anatomy. However the occipital region is slightly laterally displaced relative to the skull roof and orbitosphenoid, hampering a good fit between the olfactory tract region and the hindbrain (Figure 1, 16). The region encased by the ventral surface of the semi-cylindrical region of the orbitosphenoid bounds the cast of the olfactory bulbs and tract as well as part of the forebrain. The region enclosed by the median contact of the two parietals (pineal foramen), embrace the cast of the epiphyseal nerve. The posterior section of the skull delimited by the parasphenoid-basipresphenoid, prootics, supraoccipitals, exoccipitals and opisthotics bounds the cast of the mid- and hindbrain (Figure 1).

Although the olfactory bulbs are large, the cerebellum is still more expanded than the cerebrum (Figure 16). The olfactory bulbs are connected to the forebrain by the olfactory tract. The olfactory bulbs

are divided anteriorly by the median ridge. The orbits are located at the level of the olfactory bulbs. The connection between the cerebrum and the epiphyseal nerve is not clear because the orbitosphenoid shifted laterally relative to the parietals. However, the anterior portion of the cerebrum has an oblate ellipsoidal volume that is truncated anteriorly by the olfactory tracts.

The endocast bounded by the ventral surface of the supraoccipitals enclose symmetrical domes on the brain that may be divided by an interhemispheral fissure at the level of the sagittal supraoccipital suture (Figure 16 A).

The floccular complex lobes project posterolaterally from the cerebellum and arch dorsally (Figure 16 A). The floccular complex lobes are solely delimited by the supraoccipital, however there is an embayment on the dorsal portion of the prootics that forms a lateral inflation of the cerebellum that connects posteriorly with the floccular complex lobes (Figure 16 A, B). The total volume of the brain is ~6767mm^3.

A clear division between the forebrain and the midbrain is marked by an isthmus (Figure 16 A). The only distinguishable structure of the ventral midbrain is the hypophysis (or pituitary gland) as the optic lobes are not distinct from the hindbrain (Figure 16 B). The hypophysis is delimited by the medial process of the prootics posteriorly, and anterolaterally by the dorsum sella, forming a broad subcylindrical structure (Figure 16 B). The hypophysis is divided ventrally into two laterally-positioned pituitary lobes (Figure 16 C).

The pontine flexure marks the separation between the hindbrain and the medulla oblongata and is located posteriorly to the floccular complex lobes (Figure 16 B), contrary to the condition in dicynodonts (Castanhinha, Araújo et al. 2013).

Cranial nerves and vasculature

The epiphyseal nerve (diameter between ~2000-2300µm) exits dorsally through the pineal foramen, embraced by the parietals (Figure 16 A) and a small portion of the inferred path vena capitis dorsalis is preserved in the ventral surface of the parietal and borders the posterior half of the epiphyseal nerve (Figure 16 A). All other preserved cranial nerves exit from the ventral side of the brain (endocast) except the trigeminal nerve that exits at about mid-height of the brain (Figure 16 B) along with the vena capitis medialis between the pila antotica and the anterodorsal process of the prootic. The abducens nerve (cn VI) probably had the same path as the cerebral branch of the carotid artery (Figure 16 C). The internal carotids pierce the parasphenoid-basipresphenoid laterally and join in the median part of the skull and exits anterior to the sella turcica (Figure 16 B). This path joins with the vidian canal that runs along the laterodorsal side of the parasphenoid- basipresphenoid complex (Figure 16 B, C). A small caliber canal (diameter: ~385µm) pierces the lateral wall of the parasphenoid- basipresphenoid complex ventral to the internal carotid foramen (Figure 16 B). This canal continues horizontally and bends dorsally towards the internal carotid artery. Given the conservative pattern of the hindbrain vasculature in tetrapods this canal may be the orbital artery (Rahmat and Gilland 2014). The facial nerve (cn VII) pierces the prootic ventrolaterally oriented, and has a diameter of ~480µm (Figure 16 C). There is no osseous enclosure for the vestibulocochlear nerve (cn VIII) as the brain endocast contacts directly the medial wall of the osseous labyrinth (cf. Sigogneau 1974). The vagoaccessory and glossopharyngeal nerve (cn IX-XI) is bounded by the supraoccipital dorsally, and the opisthotic and basioccipital ventrally (Figure 16 C). The vagoaccessory and glossopharyngeal nerve exit the brain laterally right anterior to the pontine flexure, and have a diameter of ~1400µm. The osseous enclosure for the hypoglossal nerve (cn XII, Figure 16 C) exits the brain ventrolaterally and pierces the dorsal process of the basioccipital (diameter ~590µm).

DISCUSSION

We analyzed two gorgonopsian specimens, GPIT/RE/7124 and GPIT/RE/7119, using propagation phase contrast synchrotron micro-computed tomography. Our results uncovered previously unknown anatomical features of the gorgonopsian braincase that in some aspects differs from previous descriptions. We discuss below the enigmatic posterior ossification of the basisphenoid and its possible role on developmental processes and ontogeny among synapsids. In addition, we make extensive comparisons of the basicranium and occiput of GPIT/RE/7124, GPIT/RE/7119 and other published gorgonopsian specimens (Figure 17). Finally, we discuss implications of our endocranial reconstructions for sensory suite and head posture in gorgonopsians.

Ontogenetic stage of GPIT/RE/7124

Although dubious for some reptiles (Bailleul et al. 2016), among synapsids skull sutural closure is a reliable indicator of ontogenetic maturity (Dwight 1890, Todd and Lyon 1925, Krogman 1930, Schweikher 1930, Chopra 1957). Despite recent efforts to extricate ontogenetic and phylogenetic characters among gorgonopsians (Kammerer 2016), ontogenetic patterns of character change and gorgonopsian systematics remain insufficiently understood, particularly within the basicranium. Thus, it is necessary to use alternative lines of evidence such as sutural closure or bone histology to assess a relative degree of maturity among gorgonopsians. Figure 6 shows horizontal sections of the basicranial region of two ontogenetic stages in two different gorgonopsians: GPIT/RE/7124 and GPIT/RE/7119. The sutures remain visible (e.g., basipresphenoid-basipostsphenoid, prootic-basipostsphenoid, opisthotic-basioccipital, basioccipital-basipostsphenoid) and separated in GPIT/RE/7124 (Figure 6 A and B), but they are co-ossified in GPIT/RE/7119. In GPIT/RE/7119, only the opisthotic-basioccipital suture is clearly visible (Figure 17), while the rest of the sutures, although visible, are hardly distinguishable from the trabeculae mesh.

In GPIT/RE/7119, bone trabeculae are larger than in GPIT/RE/7124, indicating significant bone remodeling and resorption. It is known that the trabecular length scales with body mass (Swartz et al. 1998), and the larger specimen GPIT/RE/7119 (~20cm estimated skull length) has indeed larger trabeculae when compared to GPIT/RE/7124 (14-15cm and skull length). The incipient sutural closure and the small trabeculae of GPIT/RE/7124 are indicative of the physical immaturity (as conceptualized by Araújo et al. 2015) of this gorgonopsian specimen.

Comparative anatomy of the occiput

The occiput is a relatively conserved region in gorgonopsians, but accurate information is often inaccessible due to co-ossification of the bone elements and preservational damage. Most specimens have a concealed suture between the exoccipital and basioccipital, but also between the opisthotic and tabular, and the supraoccipital and exoccipital (Sigogneau 1970, Sigogneau-Russell 1989). As a result, there is contradictory information in previous publications concerning the formation of the occipital condyle. Olson (1938) clearly states that the occipital condyle is solely formed by the basioccipital. Conversely, Kammerer (2016) posits that the lateral portions of the occipital condyle are formed by exoccipitals. Kemp (1969) describes the exoccipital as forming the ventromedial corner of the occipital condyle. In specimens where the limits are discernible, Sigogneau (1970) and Pravoslavlev (1927) depict the exoccipitals as being excluded from the occipital condyle. Sigogneau (1970) depicts this condition in four specimens (i.e., AMNH 5515, BPI 259, IGP U 28, RC 2), but does not describe the condition specifically. Unfortunately, the occipital condyle is not preserved in GPIT/RE/7119. However, in GPIT/RE/7124 there is a clear suture visible in the tomographs separating the exoccipital from the supraoccipital and basioccipital (Figure 18). The exoccipital is completely excluded from the occipital condyle and only the ventromedial corner of the exoccipital contacts the basioccipital, somewhat resembling the condition described by Kemp, (1969), except that the basioccipital has a dorsal process

that prevents the exoccipital from contacting the occipital condyle. However, we do not rule out that some specimens might have some contribution of the exoccipital to the occipital condyle, particularly on its dorsal component (Christian Kammerer personal communication). Moreover, within the basioccipital, there is no evidence of sutures, trabeculae size variation or different types of bone (cortical versus trabecular). Importantly, there is no opisthotic-exoccipital suture, although the two bones nearly contact. These two bones are separated by the supraoccipital, despite the extension of the exoccipital lateral corner (Figure 18). Nevertheless, this feature might be different in other specimens (Christian Kammerer personal communication).

GPIT/RE/7124 can clarify the supraoccipital-interparietal relationship (Figure 18). In all serial-sectioned specimens (Olson 1938, Kemp 1969, Sigogneau 1970) the supraoccipital extends dorsally, being partially covered by the interparietal. Kemp (1969, fig. 21) and Sigogneau (1970, fig. 23, 51, 81 and 151) depict the interparietal reaching the endocranial cavity, but in laterally-shifted sagittal sections. However, in a median sagittal section, the interparietal is superficial in a variety of specimens (e.g., BPI 277, NHMUK R 4053 and RC 57) with no contact with the endocranial cavity.

Comparative anatomy of the basicranium

Although conservative in various traits, there is significant variation in the gorgonopsian basicranium. Notably, the two specimens here studied highlight variation that can be attributed to ontogeny. In agreement with previous reports (Olson 1938, Kemp 1969, Sigogneau 1970), our analysis of GPIT/RE/7124 and GPIT/RE/7119 showed that the prootics meet medially through a medial process that overlaps the basisphenoid and basioccipital. The medial contact of the prootics is apparent in the coronal section “F” in Olson (1938). This process may be more or less robust most likely depending on the ontogenetic stage. More ontogenetically advanced gorgonopsians, such as GPIT/RE/7119, show a robust and dorsoventrally expanded medial process of the prootic (Figure 17, 18B, C), whereas

GPIT/RE/7124 shows a relatively feebler medial contact and consequently a shallower depression for the hypophyseal fossa (Figure 18A, B).

The prootic has significant differences in GPIT/RE/7124 (as well as BPI 3, TMP256 and NHMUK R 5743, Sigogneau 1970) when compared to the most general pattern shown by more ontogenetically advanced specimens. GPIT/RE/7119 (Figure 17, 18B), BPI 277 (Sigogneau 1970), NHMUK R 4053 (Sigogneau 1970), BPI 290 (Sigogneau 1970), RC 60 (Sigogneau 1970), RC 34 (Sigogneau 1970), RC 103 (Sigogneau 1970) and UMZC T877 (Kemp 1969) have greatly ossified prootics. Such ontogenetic differences are expected because neurocranial elements tend to ossify later in ontogeny (Koyabu et al. 2014). In ontogenetically advanced specimens, the pila antotica is not a single rod-like structure, but instead it connects to Kemp's anterodorsal process and forms an ellipsoidal vacuity from where the trigeminal nerve and vena capitis medialis exited. However, Sigogneau (1970) and Sigogneau-Russell (1989) mistakenly identified this vacuity to form the root for the optic and oculomotor nerves. The chondrocranium in mammals has the oculomotor and trigeminal cranial nerves exiting through the same perforation of the chondrocranium (de Beer 1937, Novaceck 1993), whereas in the reptilian outgroup the optic and oculomotor cranial nerves exit anterior to the pila antotica (de Beer 1937, Bellairs and Kamal 1981, Paluh and Sheil 2013). Thus, there is no extant phylogenetic bracket supporting Sigogneau's (1970) and Sigogneau-Russell's (1989) views on the configuration and identity of the cranial nerves exiting the ellipsoidal prootic vacuity. To accept Sigogneau's (1970) configuration would imply that the anterior osseous border of the vacuity is an ossification of the planum supraseptale, and hence the orbitosphenoid. However, the anterior border of the vacuity is undoubtedly bounded by the prootic.

Probably due to poor preservation of the basicranium, the pila antotica bone identity was not clear in UCMP 42701 (Laurin 1998). Laurin (1998) stated that the pila antotica is made from a composition of various bones without specifying which. However, it is clear from the specimens studied here that the pila antotica (or Kemp's "antero-ventral" process) is part of the prootic (Figure 6, 18).

524 Nevertheless, the ossification of the pila antotica itself is unusual, and more so as part of the prootic, as
525 it has been consistently reported in the gorgonopsian literature (Olson 1944, Kemp 1969, Sigogneau
526 1970, Sigogneau-Russell 1989), as well as in various other non-gorgonopsian synapsids (e.g., Boonstra
527 1968, Cluver 1971; Fourie 1974). However, the chondrocranial pila antotica is part of the basisphenoid in
528 various amniotes (Paluh and Sheil 2013), including cynodonts (Crompton 1958, Presley and Steel 1976).
529 It is possible that the pila antotica may be part of the prootics, but there is a clear suture between the
530 parasphenoid-basipresphenoid and the prootics, particularly visible in horizontal view (Figure 6). The
531 homology/presence of the pila antotica still requires further research through morphological and
532 evolutionary interpretation of the braincase elements in more basal synapsids, as there is contradictory
533 evidence on pila antotica development in non-therapsid synapsids (see Olson 1944 versus Boonstra
534 1968). Meanwhile, the nomenclature/homology used by previous workers remains undisputed.

535 The prootic anterodorsal process does not contact the orbitosphenoid in GPIT/RE/7124 or
536 GPIT/RE/7119 (Figure 17), contrary to Kemp's (1969) interpretation for *Arctognathus*. Kemp (1969)
537 homologized the anterodorsal process to the taenia marginalis, or the parietal plate using mammalian
538 nomenclature. The taenia marginalis is the chondrocranial connection between the otic capsule and the
539 planum supraseptale (Paluh and Sheil 2013). Although the anterodorsal process is topologically located
540 on the dorsal aspect of the prootic bone (i.e., of otic capsule origin), it does not contact any osseous
541 expression of the chondrocranium anterior domain. Thus, the argument presented by Kemp (1969) and
542 followed by Sigogneau-Russell (1989) to explain the homology of the anterodorsal process is
543 questionable.

544 Importantly, there is a significant ontogenetic signal concerning the morphology and relative
545 size of the basipostsphenoid. In GPIT/RE/7124, the basipostsphenoid is a relatively important
546 component of the basicranial axis, with nearly half of the basioccipital length. However, the
547 basipostsphenoid is a minute element completely enveloped by the medial process of the prootics

548 dorsally and the basioccipital ventrally. In addition, the high degree of fusion of the basioccipital and
549 basipresphenoid renders the interpretation in such ontogenetically advanced specimens difficult.
550 Nevertheless, the clearly anterior suture of the basipostsphenoid and basioccipital in GPIT/RE/7199
551 (Figure 17), together with the more posterior larger trabeculae and the more spongious nature of the
552 bone, are indications for the separation of these bones. A similar configuration to what was observed in
553 GPIT/RE/7119 (Figure 17) was described by Olson (1938, slice "E").

554 The cerebral branch of the internal carotids has a consistent route in GPIT/RE/7124 and
555 GPIT/RE/7119 and it seems to be invariable throughout ontogeny. The cerebral branch of the internal
556 carotids pierces the wall of the parasphenoid from each side and converges medially, then perforates
557 the dorsal surface of the basipresphenoid as a single canal onto the sella turcica. Olson (1938) correctly
558 identified the internal carotids in the slice "G" and demonstrated that they pierce the lateral wall of the
559 parasphenoid (see "F" slice) but failed to show their medial convergence. Kemp (1969, fig.7) is in
560 accordance with our results.

561 We concur with the observations of Olson (1944), Kemp (1969) and Sigogneau-Russell (1989)
562 that the orbitosphenoid has two distinct ossified regions: a "postero-ventral ossification" laying on the
563 parasphenoid and an "antero-dorsal", which is continuous with the orbitosphenoid. These ossifications
564 are indeed separate in GPIT/RE/7124. In this specimen, the "postero-ventral" ossification is a small
565 portion of bone anterior to the internal carotid canal on the sella turcica, with a dome-shaped structure
566 (Figure12). The "presphenoid" of Sigogneau (1970) should be regarded as the "postero-ventral
567 ossification" of the orbitosphenoid. However, the more ontogenetically mature specimen GPIT/RE/7119
568 shows that the two ossifications are connected anteriorly but they arise from two different ossification
569 centers (Figure 17, 19E, F, G and H).

570

571 *The evolution of the synapsid basicranial axis: parabasisphenoid, prootic, basioccipital*

572 The degrees of variation and phylogenetic signal of the basicranium remain unexplored in synapsids
573 (Rougier and Wible 1995). We here compile and summarize the current knowledge on the evolution of
574 the parabasisphenoid, prootic and basioccipital complex as these bones mark a key transition between
575 the neural crest/mesoderm derived bones. It is clear, however, that further resesrch is needed, as the
576 anatomy of the basicranium is only known from few specimens of the many synapsid groups.

577 In the parareptilian outgroup, the parabasisphenoid seems to be a single element contacting the
578 basioccipital posteriorly (Spencer 2000, Tsuji 2013). However, within basal reptilians the prootics do not
579 meet medially in the procolophonids *Leptopleuron* (Spencer 2000) and *Procolophon* (Carroll and Lindsay
580 1985), the captorhinid *Eocaptorhinus* (Heaton 1979), and the basal neodiapsid *Youngina* (Gardner et al.
581 2010). The pareiasaur *Deltavjatia* appears to be an exception in displaying a medial contact (Tsuji 2013),
582 but it is possible it may result from post-mortem deformation. Extant reptilians also do not possess a
583 medial contact between the prootics (Oelrich 1956, Iordansky 1973, Gaffney 1979)

584 Among synapsids, the sphenacodontian *Dimetrodon* has a fused parabasisphenoid that contacts
585 directly the basioccipital (Romer and Price 1940, Brink and Reisz 2012). The prootics meet medially,
586 similarly to the condition in the gorgonopsians forming a structural dorsum sella (Romer and Price
587 1940). This dorsum sella formed by the prootics is not homologous to the human dorsum sella, from
588 which the term originally derived (Boele 1828), but it is a structural dorsum sella in the sense that it
589 forms the posterior wall of the hypophyseal fossa. Among therapsids, the burnetiamorph biarmosuchian
590 *Lobalopex* has a large prootic that forms the lateral wall of much of the posterior portion of the
591 braincase (Sidor et al. 2004). The hypophyseal fossa is laterally surrounded by the prootic, and the
592 prootics meet posteriorly (Sidor et al. 2004). Boonstra (1968) demonstrated for various dinocephalians
593 that the prootics meet at the midline via a process that forms the dorsal portion of the dorsum sella,
594 where the ventral portion is formed by the basisphenoid. This is also the condition observed in the
595 gorgonopsian specimens here described. However, there is no separation of the parabasisphenoid

596 complex into different ossifications in dinocephalians (Boonstra 1968). A separate ossification between
597 the basioccipital and parasphenoid-basipresphenoid has been demonstrated for the dicynodonts
598 *Niassodon* (Castanhinha, Araújo et al. 2013), *Lystrosaurus* (Cluver 1971), and it is also present in
599 GPIT/RE/9275. Dicynodonts do not have the two prootics meeting at the skull midline (Camp and Welles
600 1956, Boonstra 1968, Surkov and Benton 2004, Castanhinha, Araújo et al. 2013, Cluver 1971). The
601 prootics *crista alaris*, contacting the supraoccipital posteriorly and the pila antotica, raise anterodorsally
602 from the prootics base. This condition is seemingly a reversal from the more general condition in
603 Synapsida. It is apparent that the basicranium was under substantial morphological change among
604 therapsids, despite the limited knowledge on more basal synapsids. Therocephalians have been
605 described as possessing a midline contact of the prootics that forms the dorsum sella (Boonstra 1968,
606 1971, van den Heever 1994). From our observations for GPIT/RE/7139, the sella turcica in
607 therocephalians is anteroposteriorly elongated and the prootics contact slightly in the midline, and the
608 parabasisphenoid is a single fused element (Figure 19C, D). Further observations are required to assess
609 the ontogenetic development of the parabasisphenoid in osteologically immature specimens. The sellar
610 region in basal cynodonts has striking resemblance with that of therocephalians, with an elongated and
611 shallow sella turcica, however, the dorsum sella is shallow and formed by the basisphenoid (e.g., BP1-
612 5973 see Suppl. Video, Rigney 1938, Fourie 1974, Kemp 1979). On the other hand, the prootics are well
613 separated from one another in the sagittal plane (BP1-5973 see Suppl. Video, Rigney 1938, Fourie 1974,
614 Kemp 1979), resembling the anomodont condition. In a rare example, the synchrotron scans of
615 *Thrinaxodon liorhinus* (BP/1/7199) and *Galesaurus* (BP1-5973 see Suppl. Video) show the separation
616 between the dermal parasphenoid and the endochondral basisphenoid. A thin sheet of the
617 parasphenoid envelops the posterior portion of the basisphenoid trabecular bone. In these specimens,
618 the basisphenoid and the basioccipital are conspicuously separated by a gap [“unossified zone” of Olson
619 (1944) and Fourie (1974)]. A similar gap is filled with basal plate cartilage in other tetrapods (Paluh and

620 Sheil 2010). The basal cynodont basicranium closely resembles the mammalian condition. In the basal
621 mammaliaform *Morganucodon* (Kermack et al. 1981), or in the more derived *Triconodon* (Kermack
622 1963), the prootics are separated by a broad basisphenoid. Similarly, in mammals the petrosals/periotic
623 (prootic + opisthotic) form a rather lateral position in the braincase (Novacek 1993).

624 An important implication of the sellar region reorganization is the modification of the abducens
625 nerve path as well as the extraocular musculature, namely the retractor bulbi group. In reptiles, the
626 retractor bulbi muscles attach on the clinoid processes of the basisphenoid dorsum sella (Säve-
627 Söderbergh 1946). In mammals, on the other hand, the retractor bulbi muscles insert on the orbital
628 exposure of the basisphenoid (e.g., Porter et al. 1995). If we use the reptilian configuration as the
629 plesiomorphic condition, it follows that either the structural dorsum sella formed by the prootics medial
630 process began to serve as the attachment area of the retractor bulbi or these muscles, or that the
631 retractor bulbi inserted on a more lateral aspect of the saddle-shaped dorsal buttresses of the
632 parasphenoid-basipresphenoid tentatively homologized with the processus clinoideus (see description).
633 However, the topology of these structures does not allow us to rule out they may be the rostrum
634 basisphenoidale (Paluh and Sheil 2013). The hypothesis of attachment site adjustment from the
635 basisphenoid to the prootics medial projection does not seem to be convincing because the retractor
636 bulbi musculature has highly conservative origin loci across tetrapods (Walls 1942). On the other hand,
637 we favor the hypothesis of a small lateral readjustment of the retractor bulbi musculature towards the
638 saddle shaped buttresses on the parasphenoid-basipresphenoid complex because it is a more
639 parsimonious explanation. Otherwise, the origin of the retractor bulbi muscles would have to change
640 from the basisphenoid to the prootics in non-anomodont therapsids, and then subsequently change
641 back to the basisphenoid in mammals.

642 Although carotid circulation has been studied in detail for cynodonts and mammaliaforms
643 (Rougier and Wible 1995, Müller et al. 2011), little is known for more basal synapsids. Theriodontia

644 share a unique condition among synapsids in having the cerebral branch of the internal carotid exiting as
645 a single opening on the anteriormost portion of the sella turcica. This can be attested for GPIT/7124 and
646 GPIT/RE/7199 for gorgonopsians, GPIT/RE/7139 and van den Heever (1994) for therocephalians,
647 BP/1/7199 and Fourie (1974) for cynodonts. The condition in cynodonts and therocephalians is slightly
648 different from gorgonopsians. In cynodonts and therocephalians the two cerebral branches perforate
649 the parabasisphenoid ventrally and then subsequently coalescing at about halfway towards the dorsal
650 side of the basisphenoid, whereas in gorgonopsians the two cerebral branches perforate the
651 parabasisphenoid laterally follow a horizontal path towards the median part of the skull and then
652 coalesce at the sagittal plane. However, the parabasisphenoid region in gorgonopsians is much deeper.
653 Burnetiamorphs, dinocephalians, anomodont, but also mammaliaforms have two perforations on the
654 sella turcica for the cerebral branches of the internal carotids, thus, exiting separately (e.g., Boonstra
655 1968, Crompton 1958, Kermack 1963, Kermack et al. 1981).
656
657 *The enigmatic posterior ossification of the basisphenoid*
658 The parasphenoid-basisphenoid is a complex element in most vertebrates, formed from a number of
659 different ossifications of chondrocranial and dermatocranial origins. The complexity of this region leads
660 to nomenclatural problems arising from both homologous bones being named differently in the major
661 tetrapod groups (i.e., reptiles, birds, mammals) and evolutionary shifts in developmental programs,
662 yielding identification of homologous elements difficult (Figure 20).
663 Fate mapping experiments show a fundamental reorganization of the braincase bones among
664 vertebrates (Couly 1993, Jiang et al. 2002, Noden and Trainer 2005, Kague et al. 2012, Piekarski et al.
665 2014). For instance, the parasphenoid can be confused with the vomer (Atkins and Franz-Odendaal
666 2015), or the basipresphenoid in the chick does not seem to be homologous with the presphenoid bone

667 in the mouse (McBratney-Owen et al. 2008). It is thus, crucial to understand the therapsid origins of the
668 parasphenoid and basisphenoid to shed light on the mammalian evolution.

669 The parasphenoid and the basisphenoid are typically described separately in the gorgonopsian
670 literature (e.g., Sigogneau 1970, Sigogneau-Russell 1989, Kammerer et al. 2015, Kammerer 2016).
671 However, co-ossification of the two bones and the fact that typically only the ventral view of these
672 bones is visible, the parasphenoid refers exclusively to the cultriform process (or parasphenoid rostrum),
673 and the basisphenoid to the basal tubera, thus rendering difficulties to understand the exact
674 delimitation of each bone. Notably, the structures that compose the dorsal view of these bones have
675 not been described.

676 In the synapsid outgroup, the typical reptilian braincase configuration comprises the
677 basisphenoid which is typically fused with the cultriform process anteriorly and the lateral wings of the
678 parasphenoid ventrally (Gardner et al. 2010, Sobral et al. 2015), the degree of fusion of these elements
679 leads various authors to describe this element as the parabasisphenoid. It is consensual though that the
680 basisphenoid is perforated by the internal carotids dorsally and excavated by the sella turcica, and
681 bearing the dorsum sella posteriorly (Rieppel 1993). Lateral to the basisphenoid lay the prootics, and it is
682 often posteriorly fused with the basioccipital.

683 Importantly, the sella turcica is a highly conservative structure laying universally in vertebrates
684 on the basisphenoid (Hanken and Hall 1993). However, surprisingly, in his extensive monograph on
685 gorgonopsian anatomy Kemp (1969) described the sella turcica and the internal carotid foramina as part
686 of the parasphenoid. Indeed, the median ridge of the sella turcica are described just posterior to the
687 parasphenoid cultriform process posterior border (Kemp 1969, see fig. 7 for *Leontocephalus* and p. 64
688 for *Arctognathus*). Furthermore, he notes that the prootics have medial processes that meet in the
689 sagittal plane of the skull, thus excluding the posterior part of the parasphenoid-basisphenoid complex
690 to form the dorsum sella (similar to “pelycosaurs” Romer and Price 1940). A similar anteriorly-shifted

691 sella turcica is present in the gorgonopsian outgroup: the dicynodonts (Cluver 1971, Castanhinha, Araújo
692 et al. 2013). This unique configuration of the braincase has remained unquestioned. However, if we
693 accept that the sella turcica sits on the parasphenoid, such braincase arrangement represents a
694 dramatically different reorganization of the skull, because highly conservative structures such as the
695 sella turcica and dorsum sella modified their typical loci.
696 The separate, intermediate ossification between “Kemp’s parasphenoid” and the basioccipital in the
697 osteologically immature (see Araújo et al. 2015) skull of GPIT/RE/7124 provides significant insights into
698 the homology and ossification sequence of these structures within synapsids. The dermal bone
699 parasphenoid fuses early in ontogeny with the anterior ossification center of the basisphenoid which has
700 the neural crest-derived trabeculae as the cartilaginous precursor. The processus clinoideus and the
701 sella turcica are thus formed on the basisphenoid. The mesoderm-derived trabeculae cartilages are the
702 precursors to the posterior ossification center of the basisphenoid, which is a distinct ossification in the
703 immature GPIT/RE/7124 specimen.
704 Unexpectedly, the prootics, which originate from a different cartilaginous precursor (the otic
705 capsule), meet at the skull midline posterior to the hypophysis and the trabeculae cartilage region
706 (Figure 20). The prootics do not floor the braincase in the typical reptilian configuration (Rieppel 1993),
707 but occupy a more lateral position, the posterior part of the basisphenoid flooring the braincase. In the
708 specimen described here, the medial processes meet at the midline at the level of the posterior
709 ossification center of the basisphenoid, here called the basipostsphenoid. This explains why Kemp
710 (1969) labeled these processes the dorsum sella, due to their topological position relative to the sella
711 turcica. Thus, Kemp’s nomenclature is strictly a structural/positional term and not homologous to the
712 dorsum sella which has its chondrocranial origin as the acrochordal cartilage in various tetrapod groups
713 (Sheil 2005, Säve-Söderbergh 1946, McBratney-Owen et al. 2008, Jollie 1957, Crompton 1953).

714 Notwithstanding the developmental origins and nomenclatural aspects of the part of the bone
715 bounding the posterior part of the sella turcica, this configuration in the specimens described here
716 suggests a peculiar developmental pattern affecting the otic capsule and basal plate cartilages and was
717 widespread in the synapsid lineage. Possibly, the medial development of the otic capsule-derivative, the
718 prootics in this case, induced developmental suppression of the mesoderm-derived posterior
719 ossification center of the basisphenoid.
720

721 *The gorgonopsian brain in the context of synapsid brain evolution*

722 We here provide the first digital endocast of a gorgonopsian brain (Figure 16). In recent publications,
723 both anomodont and therocephalian endocasts provided insights on non-cynodont neotherapsids brain
724 morphology (Sigurdsen et al. 2012; Castanhinha, Araújo et al. 2013). Various publications provided also
725 pertinent information on the endocranial cavities of cynodonts (Quiroga 1980, 1984, Rodrigues et al.
726 2013). However, the critical phases of the synapsid brain evolution happened later in two pulses
727 exemplified by the endocasts of *Morganucodon* and *Hadrocodium* (Rowe et al. 2011). Neither
728 anomodonts (Castanhinha , Araújo et al. 2013), nor gorgonopsians (this paper), nor therocephalians
729 (Sigurdsen et al. 2012) show any signs of the expansion of the neocortex and elevated encephalization
730 coefficients to mammalian levels. Indeed, our findings support that pre-mammaliaform brain
731 morphology and volume remained conservative, even among derived cynodonts (Ulinsky 1986,
732 Rodrigues et al. 2013, Rowe et al. 2011). Indeed, the enlarged hindbrain relative to the forebrain, the
733 large epiphyseal nerve, the large hypophysis, and the elongate shape of the brain endocast are
734 conservative among non-mammaliaform neotherapsids, sharing a more general aspect with a reptilian-
735 grade brain. However, some derived features visible in basal cynodonts are not present in the
736 gorgonopsian representation here provided, namely the anterior colliculi (Quiroga 1980).

737 Kemp (1969) attempted to reconstruct the brain endocast from a variety of different specimens
738 from different species, rendering difficult direct comparisons with the endocast described here.
739 However, some differences from our reconstruction are conspicuous, namely in the hypophysis and
740 epiphyseal nerve. The brain endocast of GPIT/RE/7124 differs from that of Kemp (1969) as he
741 reconstructed a highly-elongated, posteriorly-oriented hypophysis. The GPIT/RE/7124 hypophysis
742 endocast is vertically-oriented and a rather short and stout depression in the basipresphenoid.

743 There is no evidence of a parapineal organ anterior to the pineal organ, as suggested by Kemp
744 (1969). The epiphyseal nerve in GPIT/RE/7124 exits through a single oval opening bounded by the
745 parietals. Additionally, Kemp (1969) estimates the exit of the optic nerve (cnII) near the junction
746 between the forebrain and midbrain. However, as he noted for his specimens, there is also no evidence
747 in GPIT/RE/7124 for any osseous enclosure of the optic nerve.

748 The floccular complex lobes are proportionally large compared with the estimated brain
749 endocast volume in the gorgonopsian taxon studied here. However, a recent study showed that ecology
750 or function does not correlate with floccular size (Ferreira-Cardoso et al. in press). Although
751 morphologically well-delimited, the flocculus is not functionally compartmentalized, but it is rather a
752 functionally-integrated structure with the rest of the cerebellum, notably for gaze stabilization and
753 vestibule-ocular reflex (Ferreira-Cardoso et al. in press).

754

755 *Osseous labyrinth*

756 Olson (1938, 1944) was the first to study the inner ear of gorgonopsians. The anatomy of the model of
757 the membranous labyrinth presented by Olson (1938) is substantially different from the endocast
758 presented here (Figure 21). For instance, the extensive development of the ampullae, the anterior and
759 posterior semicircular canals being subequal in size, there is a high degree of torsion of the horizontal

semicircular canal, and the crus communis is subtriangular in shape tapering dorsally (Olson 1938, fig. 2). Furthermore, most of the features described on the membranous labyrinth (e.g., utriculus, sacculus) cannot be discerned from the osseous enclosure of the labyrinth. However, a second attempt was performed by Sigogneau (1974) also using serial grinding techniques to reconstruct the osseous labyrinth of *Gorgonops* (BP/1/277). Although the model resulting from the grinding techniques does not seem to be in total accordance with ours (e.g., development of the ampullae, location and development of the osseous enclosure of the utriculus and sacculus, "doubling" of the anterior semicircular canal, the osseous enclosure of the labyrinth done by the opisthotic exclusively), various observations done by Sigogneau (1974) and Sigogneau-Russell (1989) are in agreement with our findings (Figure 21). Notably, the oblique orientation of the entire vestibular organ with respect to the cranial axis, the absence of ossification of the horizontal semicircular canal, the partially open canal of the anterior semicircular canal, poor development of the osseous enclosure of the ampullae, and the longer anterior semicircular canal relative to the posterior (Figure 21, Sigogneau 1974, Sigogneau-Russell 1989).

Head posture in gorgonopsians

The orientation of the horizontal semicircular canal has been used to estimate the habitual alert head posture (Lebedkin 1924, Duijm 1951, Rogers, 1998, Evans, 2006). Although questions have been raised concerning this assumption (Marugán-Lobón et al. 2013), even in the extreme case of the sauropod *Nigerasaurus,* the head is still tilted forward after the Procrustes methods proposed by the authors had been applied. Indeed, most authors agree that the alert posture requires a leveled horizontal semicircular canal or slightly elevated in the front in about 5-10° (Lebedkin 1924, Duijm 1951, Erichsen et al. 1989, Witmer et al. 2003). If the horizontal semicircular canal is aligned relative to the earth's surface plane, this implies that the head of GPIT/RE/7124 is tilted by 41° (Figure 22). This ventrally-tilted

head posture has been related to binocular vision, allowing for a greater overlap of the visual fields (Witmer et al. 2003), consistent with the predatory habits of gorgonopsians.

The closed osseous enclosure of the horizontal semicircular canal

The horizontal semicircular canal is discoid instead of the typical toroid shape (Figure 21). This is consistent in both sides of the skull, and was also reported in *Gorgonops* by Sigogneau (1974), and suggests we can rule out skull deformation and distortion to explain this unique anatomy, unique amongst reptiles.

The functional implications of this distinctive morphology are difficult to understand. The membranous labyrinth typically runs close to the inner wall of the bony labyrinth; therefore, it seems unlikely that the membranous labyrinth occupied a deeper position.

The horizontal semicircular canal lays in a deep excavation on the dorsal surface of the opisthotic (Figure 9) and there is a similarly deep excavation in the dorsal surface of the supraoccipital (Figure 10). Therefore, the horizontal semicircular canal is wedged in between these two bones. Arguably, spatial or possibly developmental constraints (or both) prevent the typical toroidal configuration of the horizontal semicircular canal.

Acknowledgements

The authors would like to thank Philip Havlik and Madelaine Böhme for the specimen loan (GPIT). Valuable comments from Christian Kammerer and an anonymous reviewer improved the manuscript substantially. RA would also like to thank Pierre-Olivier Antoine and Laurent Marivaux for continuous support.

References

807 Angielczyk, K.D., Steyer, J.S., Sidor, C.A., Smith, R.M., Whatley, R.L. and Tolan, S., 2014. Permian and
808 Triassic dicynodont (Therapsida: Anomodontia) faunas of the Luangwa Basin, Zambia: taxonomic update
809 and implications for dicynodont biogeography and biostratigraphy. In Early evolutionary history of the
810 Synapsida (pp. 93-138). Springer Netherlands.
811
812 Araújo R., Lindgren J., Polcyn M. J., Jacobs L. L., Schulp A. S., Mateus O. (2015). New aristonectine
813 elasmosaurid plesiosaur specimens from the Early Maastrichtian of Angola and comments on
814 paedomorphism in plesiosaurs. Netherlands Journal of Geosciences - Geologie en Mijnbouw. 94(1): 93-
815 108 doi: 10.1017/njg.2014.43
816
817 Atkins, J.B. and Franz-Odendaal, T.A., 2015. The evolutionary and morphological history of the
818 parasphenoid bone in vertebrates. Acta Zoologica. 97:255-263.
819
820 Bailleul AM, Scannella JB, Horner JR, Evans DC (2016) Fusion Patterns in the Skulls of Modern Archosaurs
821 Reveal That Sutures Are Ambiguous Maturity Indicators for the Dinosauria. PLoS ONE 11(2): e0147687.
822 doi:10.1371/journal.pone.0147687
823
824 de Beer GR. 1937. The Development of the Vertebrate Skull. Oxford: Oxford University Press.
825
826 Bellairs A d'A, Kamal AM. 1981. The chondrocranium and the development of the skull in recent reptiles.
827 In: Gans C, Parsons TS, editors. Biology of the Reptilia, Vol. 11: Morphology. London: Academic Press.
828 pp.1–263.
829

830 Boele, A. (1828). Dissertatio pathologica inauguralis De vermibus intestinalibus, in viis biliferis repertis.
831 Trajecti ad Rhenum: typis mandavit N. van der Monde.
832
833 Boonstra, L.D., 1968. The braincase, basicranial axis and median septum in the Dinocephalia. Ann South
834 Afr Mus 50: 195–273
835
836 Boonstra, L. D. 1971. The early therapsids. Annals of the South African Museum 59: 17-46.
837
838 Brink, K.S. and Reisz, R.R., 2012. Morphology of the palate and braincase of *Dimetrodon milleri*.
839 Historical Biology, 24(5):453-459.
840
841 Camp CL, Welles SP (1956) Triassic dicynodont reptiles. Part I. The North American genus *Placerias*.
842 Berkeley: University of California Press. 255–304 p.
843
844 Carroll, R.L. and Lindsay, W., 1985. Cranial anatomy of the primitive reptile *Procolophon*. Canadian
845 Journal of Earth Sciences, 22(11): 1571-1587.
846
847 Castanhinha R., Araújo R., Júnior L. C., Angielczyk K. D., Martins G. G., Rui M. S. Martins, C. Chaouiya, F.
848 Beckmann, F. Wilde (2013) Bringing Dicynodonts Back to Life: Paleobiology and anatomy of a new
849 emydopoid genus from the Upper Permian of Mozambique. PLoS ONE 8(12): e80974.
850 doi:10.1371/journal.pone.0080974.
851
852 Chopra SRK. The cranial suture closure in monkeys; 1957. Wiley Online Library. pp. 67–112.
853

854 Cluver M (1971) The cranial morphology of the dicynodont genus *Lystrosaurus*. Ann South Afr Mus 56:
855 155–274.
856
857 Cohen, K.M., Finney, S.C., Gibbard, P.L. & Fan, J.-X. (2013; updated) The ICS International
858 Chronostratigraphic Chart. Episodes 36: 199-204.
859
860 Couly, G.F., Coltey, P.M. and Le Douarin, N.M., 1993. The triple origin of skull in higher vertebrates: a
861 study in quail-chick chimeras. Development, 117(2), pp.409-429.
862
863 Crompton, A.W., 1953. The development of the chondrocranium of *Spheniscus demersus* with special
864 reference to the columella auris of birds. Acta Zoologica, 34(1-2), pp.71-146.
865
866 Crompton, A.W. and Museum, S.A., 1958, March. The cranial morphology of a new genus and species of
867 ictidosauran. Proceedings of the Zoological Society of London 130(2):183-216.
868 Duijm, M., 1951. On the head posture in birds and its relation to some anatomical features: I-II.
869 Proceedings of the Koninklijke Nederlandse Akademie van Wetenschappen, Series C, 54, pp.260-271.
870
871 Dwight T (1890) The closure of the cranial sutures as a sign of age. The Boston Medical and Surgical
872 Journal 122: 389–392. doi: 10.1056/nejm189004241221701.
873
874 Erichsen, J.T., Hodos, W., Evinger, C., Bessette, B.B. and Phillips, S.J., 1989. Head orientation in pigeons:
875 postural, locomotor and visual determinants. Brain, behavior and evolution, 33(5), pp.268-278.
876

877 Evans DC. 2006. Nasal cavity homologies and cranial crest function in Lambeosaurine Dinosaurs.
878 Paleobiology 32:109-125.
879
880 Ferreira-Cardoso, S., Araújo, R., Martins, N.E., Martins, G.G., Walsh, S., Martins, R.M.S, Kardjilov, N.,
881 Manke, I., Hilger, A. and Castanhinha, R. (in press). Floccular complex lobes size is not a reliable proxy of
882 ecology and behavior of fossil vertebrates. Scientific Reports.
883
884 Fourie, S., 1974. The cranial morphology of *Thrinaxodon liorhinus* Seeley. Annals of the South African
885 Museum 65:337-400.
886
887 Gaffney, E.S., 1979. Comparative cranial morphology of recent and fossil turtles. American Museum of
888 Natural History. 164(2): 65-376.
889
890 Gardner, Nicholas M., Holliday, Casey M., and O'Keefe, F. Robin, 2010. The braincase of *Youngina*
891 *capensis* (Reptilia, Dipsida): new insights from high-resolution ct scanning of the holotype Palaeontologia
892 Electronica Vol. 13, Issue 3; 19A:16p; http://palaeoelectronica.org/2010_3/217/index.html
893
894 Gebauer, E.V., 2007. Phylogeny and Evolution of the Gorgonopsia with a Special Reference to the Skull
895 and Skeleton of GPIT/RE/7113 (*'Aelurognathus?'parringtoni*) (Doctoral dissertation, Universität
896 Tübingen).
897
898 Hanken, J. and Hall, B. K. 1993. The Skull. Volume 2. Patterns of structural and systematic diversity.
899 Univrsity of Chicgo Press, Chicago. 566p.
900

901 Heaton, M.J., 1979. Cranial anatomy of primitive captorhinid reptiles from the Late Pennsylvanian and
902 Early Permian, Oklahoma and Texas. Bulletin of the Oklahoma Geological Survey 127:1-84
903
904 van den Heever, J.A.,van den 1994.Thecranialanatomy of the early Therocephalia (Amniota: Therapsida).
905 Annals University of Stellenbosch 1: 1–59.
906
907 Huene, F.V., 1937. Drei Theriodontier-Schâdel aus Sùdafrica. Pal. Zeit, 19(3-4), pp.297-315.
908 Säve-Söderbergh, G., 1946. On the fossa hypophyseos and the attachment of the retractor bulbi group
909 in *Sphenodon*, *Varanus*, and *Lacerta*. Arkiv för Zoologi, 38(11):1-24.
910
911 Iordansky, N.N., 1973. The skull of the Crocodilia. In: Gans, C. (Ed.), Biology of the Reptilia, Vol. 4.
912 Morphology D. Academic Press, London, pp. 201-262.
913
914 Jiang, X., Iseki, S., Maxson, R.E., Sucov, H.M. and Morriss-Kay, G.M., 2002. Tissue origins and interactions
915 in the mammalian skull vault. Developmental biology, 241(1), pp.106-116.
916
917 Jollie, M.T., 1957. The head skeleton of the chicken and remarks on the anatomy of this region in other
918 birds. Journal of Morphology, 100(3), pp.389-436.
919
920 Jones, Marc E.H., Curtis, Neil, Fagan, Michael J., O'Higgins, Paul and Evans,Susan E. 2011. Hard tissue
921 anatomy of the cranial joints in *Sphenodon* (Rhynchocephalia): sutures, kinesis, and skull mechanics.
922 Palaeontologia Electronica Vol. 14, Issue 2; 17A:92p; palaeo-electronica.org/2011_2/251/index.html
923

924 Kague, E., Gallagher, M., Burke, S., Parsons, M., Franz-Odendaal, T. and Fisher, S., 2012. Skeletogenic
925 fate of zebrafish cranial and trunk neural crest. PLoS One, 7(11), p.e47394.
926
927 Kammerer CF. 2014. A redescription of *Eriphostoma microdon* Broom, 1911 (Therapsida, Gorgonopsia)
928 from the Tapinocephalus Assemblage Zone of South Africa and a review of Middle Permian
929 gorgonopsians. In: Kammerer CF, Angielczyk KD, Fröbisch J, eds. Early Evolutionary History of the
930 Synapsida. Dordrecht: Springer. 171-184 337 pp
931
932 Kammerer CF. 2015. Cranial osteology of *Arctognathus curvimola*, a short-snouted gorgonopsian from
933 the Late Permian of South Africa. Papers in Palaeontology 1:41-58
934
935 Kammerer, C.F., Smith, R.M., Day, M.O. and Rubidge, B.S., 2015. New information on the morphology
936 and stratigraphic range of the mid-Permian gorgonopsian *Eriphostoma microdon* Broom, 1911. Papers in
937 Palaeontology, 1(2), pp.201-221.
938
939 Kammerer CF. (2016) Systematics of the Rubidgeinae (Therapsida: Gorgonopsia) PeerJ 4:e1608
940 https://doi.org/10.7717/peerj.1608
941
942 Kermack, K.A., 1963. The cranial structure of the triconodonts. Philosophical Transactions of the Royal
943 Society B: Biological Sciences, 246(727):83-103.
944
945 Kermack, K.A., Mussett, F. and Rigney, H.W., 1981. The skull of *Morganucodon*. Zoological Journal of the
946 Linnean Society, 71(1):1-158.
947

948 Kemp TS. 1969. On the functional morphology of the gorgonopsid skull. Philosophical Transactions of
949 the Royal Society of London, Series B, Biological Sciences 256:1-83
950
951 Kitching, J. W. 1977. The Distribution of the Karroo Vertebrate Fauna: With Special
952 Reference to certain genera and the bearing of this distribution on the zoning of
953 the Beaufort Beds, Bernard Price Institute for Palaeontological Research,
954 University of the Witwatersrand.
955
956 Krogman W (1930) Studies in growth changes in the skull and face of anthropoids. II. Ectocranial and
957 endocranial suture closure in anthropoids and Old World Apes. American Journal of Anatomy 46: 315–
958 353. doi: 10.1002/aja.1000460206
959
960 Koyabu, D., Werneburg, I., Morimoto, N., Zollikofer, C.P., Forasiepi, A.M., Endo, H., Kimura, J., Ohdachi,
961 S.D., Son, N.T. and Sánchez-Villagra, M.R., 2014. Mammalian skull heterochrony reveals modular
962 evolution and a link between cranial development and brain size. Nature communications, 5.
963
964 Laurin M. 1998. New data on the cranial anatomy of *Lycaenops* (Synapsida, Gorgonopsidae), and
965 reflections on the possible presence of streptostyly in gorgonopsians. Journal of Vertebrate
966 Paleontology 18:765-776
967
968 Lebedkin S. 1924. Uber die Lage des Canalis semicircularis bei Säugern. Anatonzischer Anzeiger 58:449-
969 460
970

971 Marugán-Lobón J, Chiappe LM, Farke AA. (2013) The variability of inner ear orientation in saurischian
972 dinosaurs: testing the use of semicircular canals as a reference system for comparative anatomy. PeerJ
973 1:e124 https://doi.org/10.7717/peerj.124
974
975 McBratney-Owen, B., Iseki, S., Bamforth, S.D., Olsen, B.R. and Morriss-Kay, G.M., 2008. Development
976 and tissue origins of the mammalian cranial base. Developmental biology, 322(1), pp.121-132.
977
978 Mirone A, Brun E, Gouillart E, Tafforeau P,Kieffer J. 2014 The PyHST2 hybrid distributed code for high
979 speed tomographic reconstruction with iterative reconstruction and a priori knowledge capabilities.
980 Nucl. Instr. Meth. Phys. Res. 324, 41-48.
981
982 Müller, J., Sterli, J. and Anquetin, J., 2011. Carotid circulation in amniotes and its implications for turtle
983 relationships. Neues Jahrbuch für Geologie und Paläontologie-Abhandlungen, 261(3):289-297.
984
985 Noden, D.M. and Trainor, P.A., 2005. Relations and interactions between cranial mesoderm and neural
986 crest populations. Journal of anatomy, 207(5), pp.575-601.
987
988 Novacek, M.J. 1993. Patterns of diversity in the mammalian skull. In The skull, Vol. 2 (ed. J.H. Hanken
989 and B.K. Hall), pp. 438-546. The University of Chicago Press, Chicago, 11.
990
991 Oelrich, T., 1956. The anatomy of the head of *Ctenosaura pectinata* (Iguan idae). Misc . Publ. Mus. Zool.,
992 Univ. Michigan 94:1-122.
993

994 Olson, E. C. 1938a. The occipital, otic, basicranial and pterygoid regions of the Gorgonopsia. J. Morph.
995 62: 141-175.
996
997 Olson, E. C. 1944 The origin of mammals based upon the cranial morphology of the therapsid suborders.
998 Spec. Pap. Geol. Soc. Am. 55, 1.
999
1000 Paganin D, Mayo S, Gureyev TE, Miller PR,Wilkins SW. 2002 Simultaneous phase and amplitude
1001 extraction from a single defocused image of a homogeneous object. Journal of microscopy 206(1), 33-
1002 40.
1003
1004 Paluh, D. J. and Sheil, C. A., 2013. Anatomy of the fully formed chondrocranium of *Emydura subglobosa*
1005 (Chelidae): A pleurodiran turtle. Journal of morphology, 274(1):1-10.
1006
1007 Parrington, F. R. 1955 On the cranial anatomy of some gorgonopsids and the synapsid middle ear. Proc.
1008 zool. Soc. Lond. 125, 1.
1009
1010 Piekarski, N., Gross, J.B. and Hanken, J., 2014. Evolutionary innovation and conservation in the
1011 embryonic derivation of the vertebrate skull. Nature communications, 5.
1012
1013 Porter, J.D., Baker, R.S., Ragusa, R.J. and Brueckner, J.K., 1995. Extraocular muscles: basic and clinical
1014 aspects of structure and function. Survey of ophthalmology, 39(6), pp.451-484.
1015
1016 Pravoslavlev, P. A. (1927). Gorgonopsidae from the North Dvina Expedition of V. P. Amalitzki. Severo-
1017 Dvinskie raskopki Prof. V. P. Amalitskogo, 3, 1–117 [in Russian].

1018

1019 Presely, R. and Steel, F.L., 1976. On the homology of the alisphenoid. Journal of anatomy, 121(3):441-

1020 459.

1021

1022 Quiroga, J.C., 1980. The brain of the mammal-like reptile *Probainognathus jenseni* (Therapsida,

1023 Cynodontia). A correlative paleo-neoneurological approach to the neocortex at the reptile-mammal

1024 transition. Journal fur Hirnforschung, 21(3):299-336.

1025

1026 Quiroga, J.C., 1984. The endocranial cast of the advanced mammal-like reptile *Therioherpeton cargnini*

1027 (Therapsida-Cynodontia) from the Middle Triassic of Brazil. Journal fur Hirnforschung, 25(3):285-290.

1028

1029 Rahmat, S. and Gilland, E., 2014. Comparative Anatomy of the Carotid-Basilar Arterial Trunk and

1030 Hindbrain Penetrating Arteries in Vertebrates. The Open Anatomy Journal, 6(1).

1031

1032 Rieppel, O., 1993. Patterns of diversity in the reptilian skull. The skull, 2, pp.344-390.

1033

1034 Rigney, H.W., 1938. The morphology of the skull of a young *Galesaurus planiceps* and related forms.

1035 Journal of Morphology, 63(3), pp.491-529.

1036

1037 Romer, A.S. and Price, L.W., 1940. Review of the Pelycosauria. Geological Society of America Special

1038 Papers, 28, pp.1-534.

1039

1040 Rogers SW. 1998. Exploring dinosaur neuropaleobiology: viewpoint computed tomography scanning and

1041 analysis of an Allosaurus fragilis endocast. Neuron 21:673-679

1042

1043 Rougier GW, Wible JR. 2006. Major changes in the ear region and basicranium of early mammals. In:

1044 CarranoMT, GaudinTJ, BlobRW, WibleJR, editors. Amniote paleobiology: perspectives on the evolution

1045 of mammals, birds, and reptiles. Chicago: University of Chicago Press. p 269–311.

1046

1047 Rubidge, B.S., Erwin, D.H., Ramezani, J., Bowring, S.A. and de Klerk, W.J., 2013. High-precision temporal

1048 calibration of Late Permian vertebrate biostratigraphy: U-Pb zircon constraints from the Karoo

1049 Supergroup, South Africa. Geology, 41(3), pp.363-366.

1050

1051 Rowe TB, Macrini TE, Luo Z-X (2011) Fossil evidence on origin of the mammalian brain. Science 332:

1052 955–957. doi: 10.1126/science.1203117

1053

1054 Säve-Söderbergh,G.(1946).Onthefossahypophyseosandtheattachmentoftheretractor

1055 bulbi group in *Sphenodon*, *Varanus* and *Lacerta*. Arch. Zool., Stockholm 38, 1–24

1056

1057 Schweikher F (1930) Ectocranial suture closure in the hyaenas. American Journal of Anatomy 45: 443–

1058 460. doi: 10.1002/aja.1000450305

1059

1060 Sidor, C.A., Hopson, J.A. and Keyser, A.W., 2004. A new burnetiamorph therapsid from the Teekloof

1061 Formation, Permian, of South Africa. Journal of Vertebrate Paleontology, 24(4):938-950.

1062

1063 Sigogneau D. 1970. Révision systématique des gorgonopsiens sud-africains. In: Cahiers de Paléontologie.

1064 Paris: Centre National de la Recherche Scientifique. 417 pp

1065

1066 Sigogneau, D., 1974. The inner ear of *Gorgonops* (Reptilia, Therapsida, Gorgonopsia). Ann S Afr Mus, 64,
1067 pp.53-69.
1068
1069 Sigogneau-Russell D. 1989. Theriodontia I. In: Handbuch der Paläoherpetologie. Stuttgart: Gustav Fischer
1070 Verlag.
1071
1072 Spencer, P. S. 2000. The braincase structure of *Leptopleuron lacertinum* Owen (Parareptilia:
1073 Procolophonidae). Journal of Vertebrate Paleontology 21, 21–30.
1074
1075 Sheil, C.A., 2005. Skeletal development of *Macrochelys temminckii* (Reptilia: Testudines: Chelydridae).
1076 Journal of Morphology, 263(1), pp.71-106.
1077
1078 Sobral, G., Sues, H.D. and Müller, J., 2015. Anatomy of the enigmatic reptile *Elachistosuchus huenei*
1079 Janensch, 1949 (Reptilia: Diapsida) from the Upper Triassic of Germany and its relevance for the origin
1080 of Sauria. PloS one, 10(9), p.e0135114.
1081
1082 Surkov, M.V. and Benton, M.J., 2004. The basicranium of dicynodonts (Synapsida) and its use in
1083 phylogenetic analysis. Palaeontology, 47(3):619-638.
1084
1085 Romer, A. S. & Price, L. W. 1940 Review of the Pelycosauria. Spec. Pap. Geol. Soc. Am. 28, 1.
1086
1087 Todd TW, Lyon D (1925) Cranial suture closure. Its progress and age relationship. Part II.—Ectocranial
1088 closure in adult males of white stock. American Journal of Physical Anthropology 8: 23–45. doi:
1089 10.1002/ajpa.1330080103

Tsuji, L.A., 2013. Anatomy, cranial ontogeny and phylogenetic relationships of the pareiasaur *Deltavjatia rossicus* from the Late Permian of central Russia. Earth and Environmental Science Transactions of the Royal Society of Edinburgh, 104(02):81-122.

Ulinski, P.S. 1986. Neurobiology of the therapsid-mammal transition. In The Ecology and Biology of Mammal-like Reptiles, ed. N. Hotton III, P.B. Maclean, J.J. Roth, and E.C. Roth, 149–171. Washington, DC Smithsonian.

van der Walt, M., Day, M., Rubidge, B., Cooper, A.K. and Netterberg, I., 2010. A new GIS-based biozone map of the Beaufort Group (Karoo Supergroup), South Africa. Palaeont. afr. 45: 1–5

Walls, G. L. (1942). The Vertebrate Eye and its Adaptive Radiation (pp. 785). Reprinted 2013. Mansfield Centre: Martino Publishing.

Witmer, L.M., Chatterjee, S., Franzosa, J. and Rowe, T., 2003. Neuroanatomy of flying reptiles and implications for flight, posture and behaviour. Nature, 425(6961), pp.950-953.

1108 **Figures**

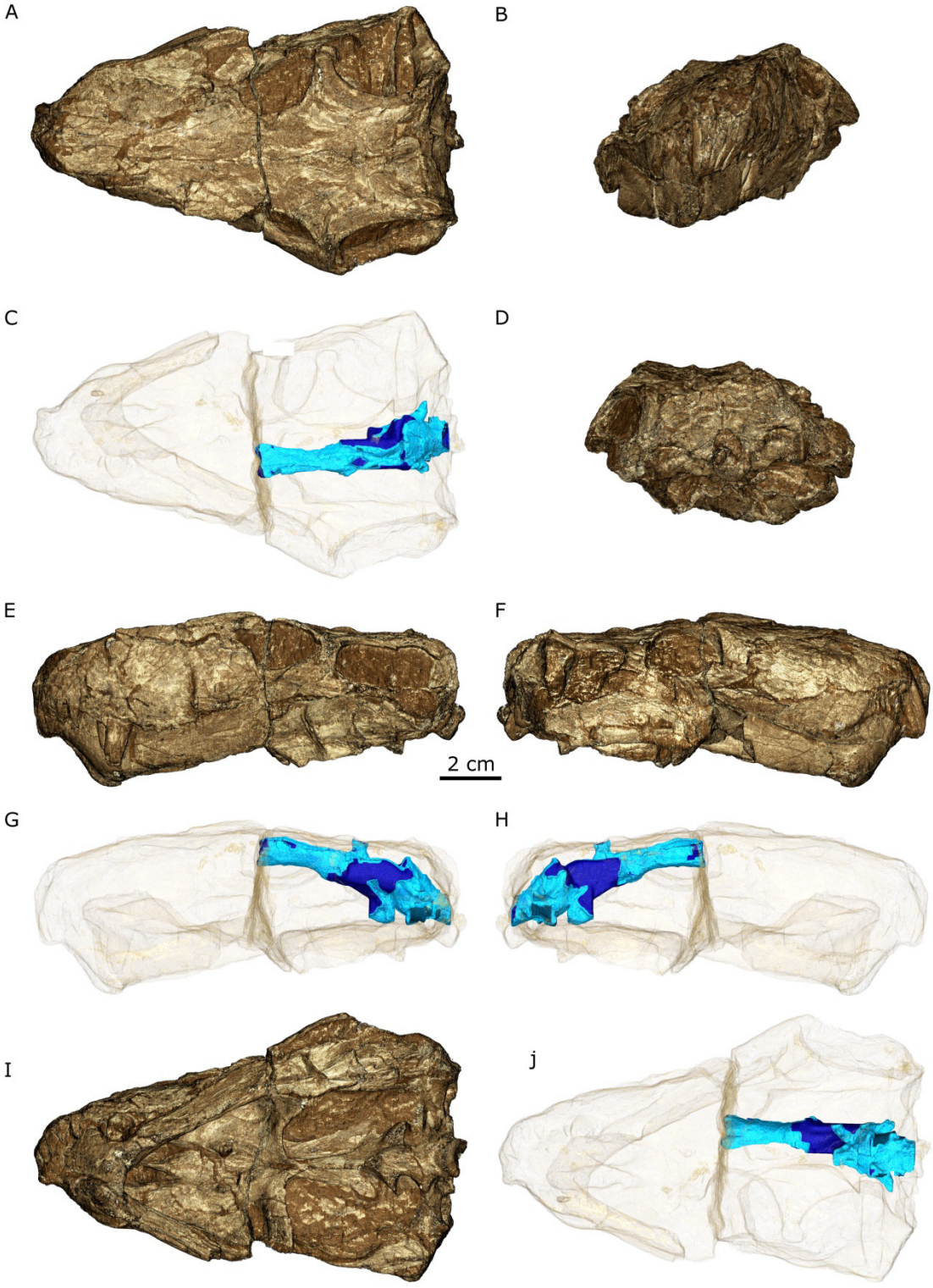

1109

Figure 1 – Three dimension rendering of GPIT/RE/7124 skull in dorsal (A), anterior (B), posterior (D), lateral left (E) and right (F) and ventral (H) view. Semi-transparent rendering of the skull with endocast (blue) in dorsal (C), lateral left (G) and right (H) and ventral (J) view. The light blue color of the endocast indicates where the segmentation was surrounded by bones unlike the dark blue parts.

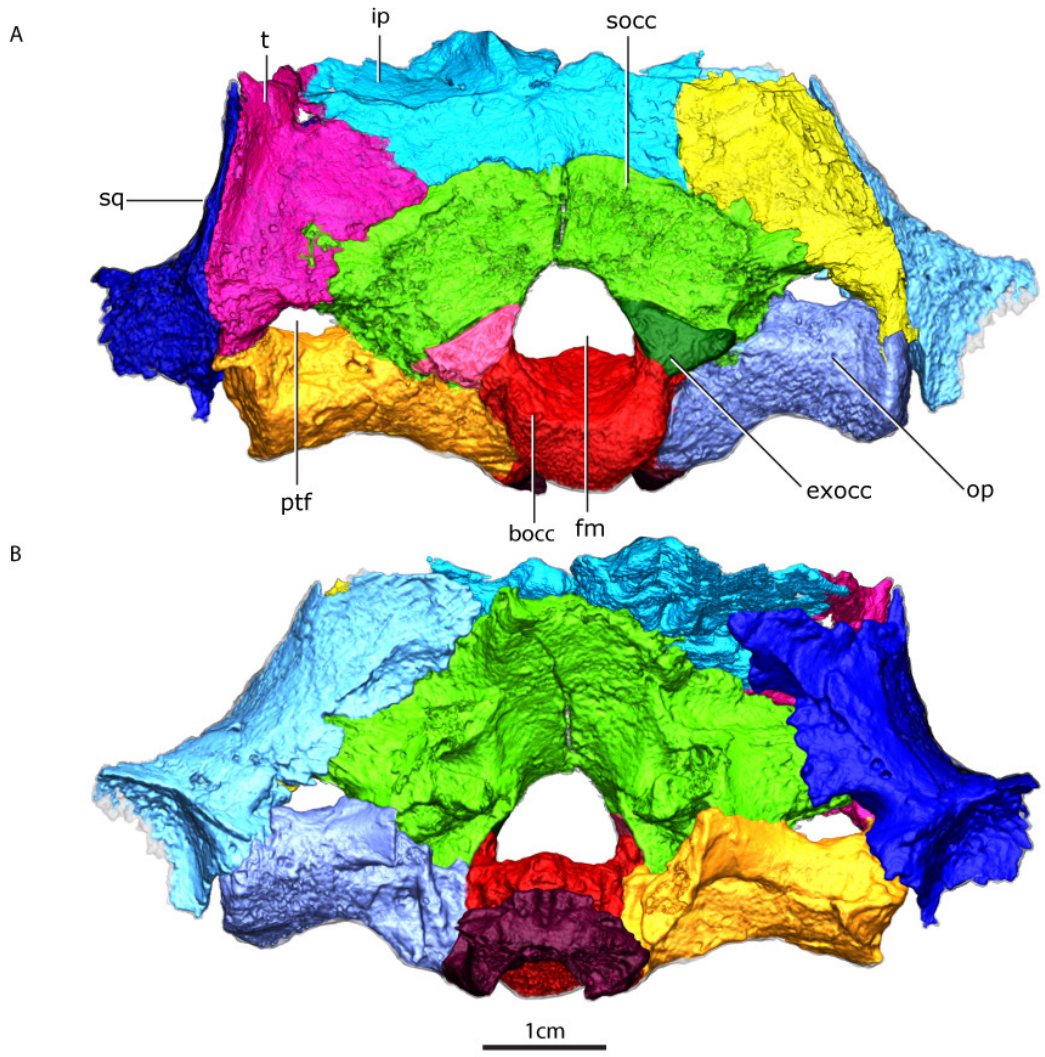

Figure 2 – Occiput in posterior (A) and anterior view (B). Abbreviations: bocc – basioccipital, exocc – exoccipital, fm – foramen magnum, ip – interparietal, jf – jugular foramen, op – opisthotic, ptf – posttemporal fenestra, socc – supraoccipital, sq – squamosal, t – tabular

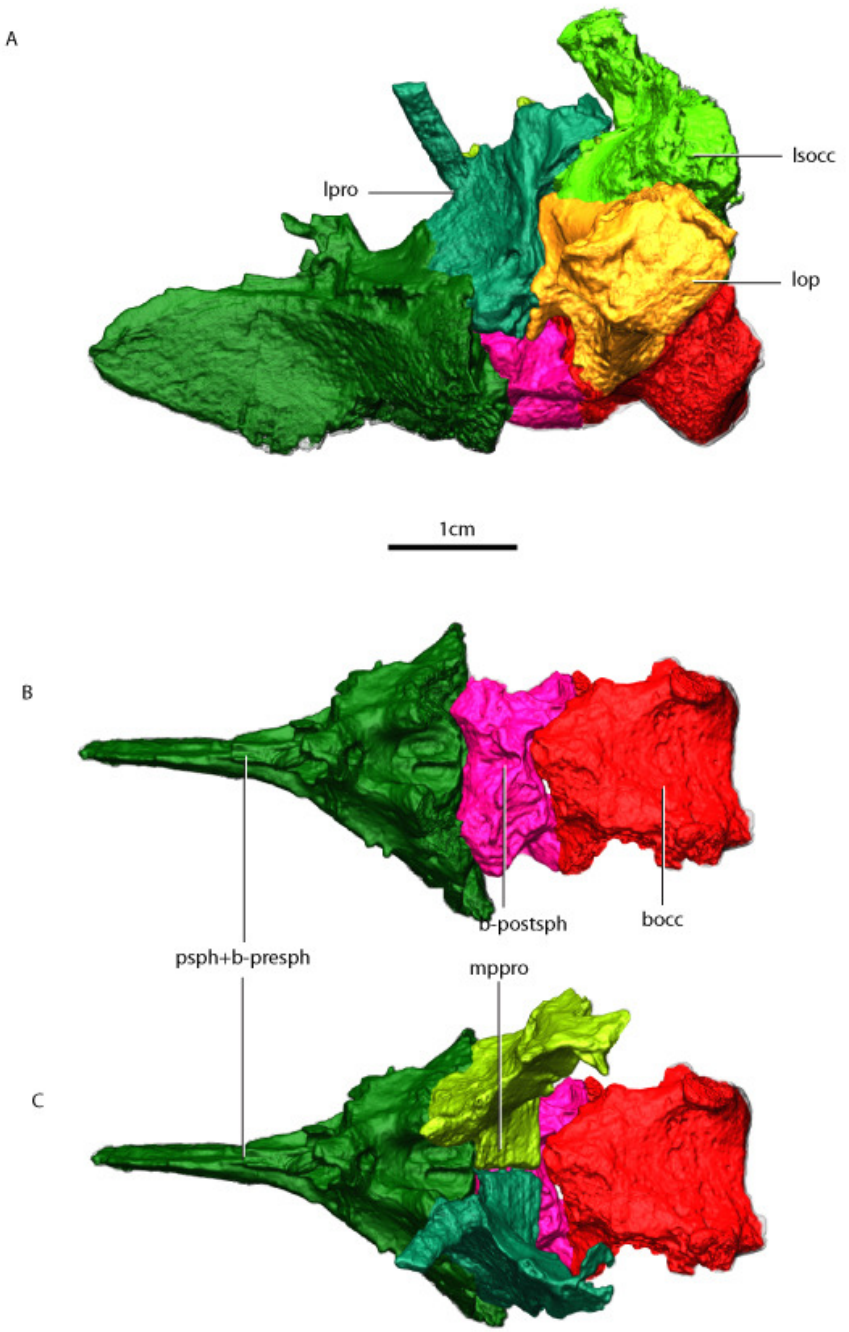

1118

1119

1120 Figure 3 – Topological arrangement of the basicranial elements in lateral (A), dorsal (B, C) views, with

1121 the parasphenoid-basipresphenoid complex anteriorly, then the basipostsphenoid overlaid by the

1122 medial process of the prootics (C), which are posteriorly bounded by the basioccipital. Abbreviations:

1123 lpro – left prootic, socc - supraoccipital

1124

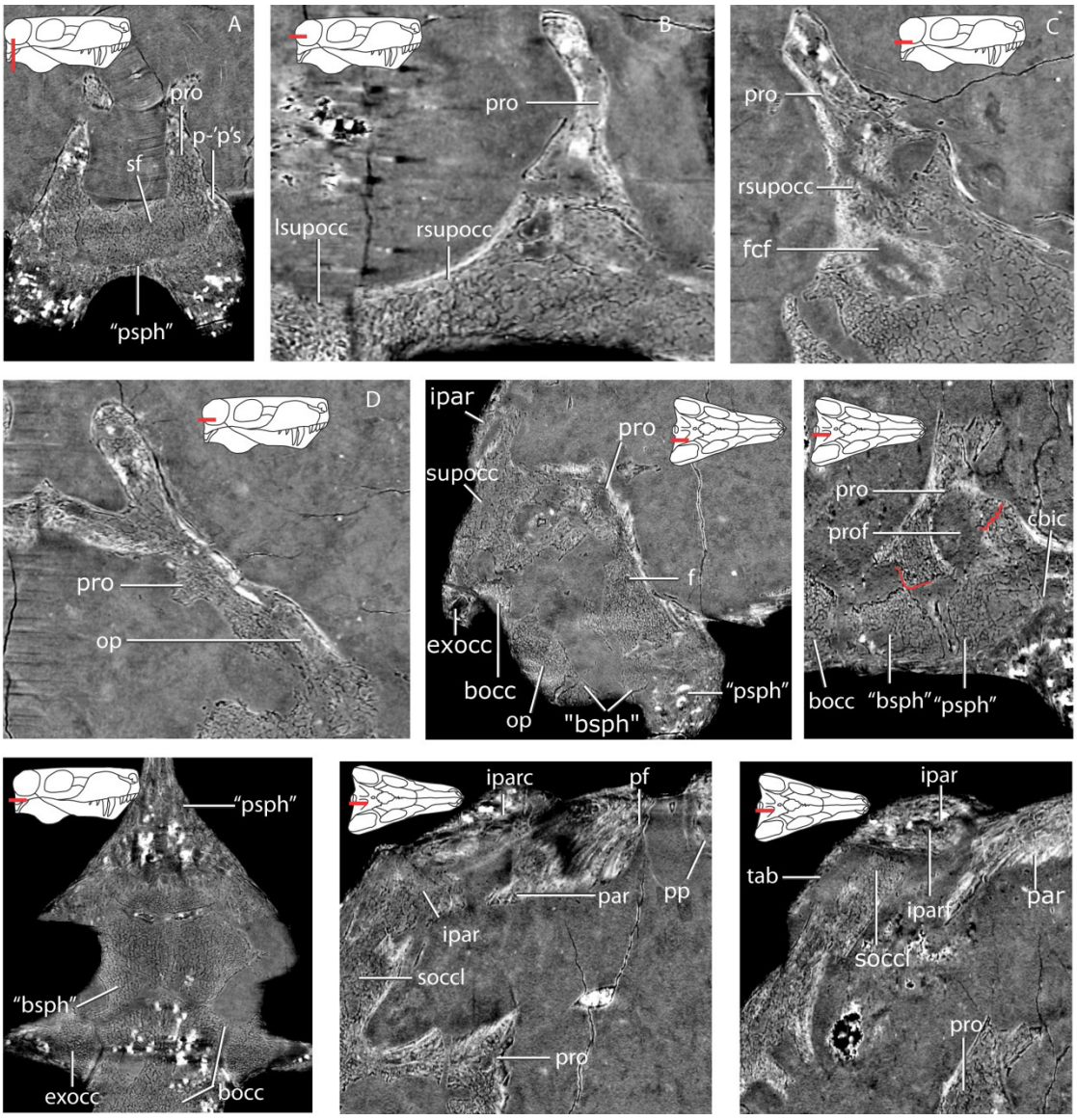

1125

1126 Figure 4 - A - the "parasphenoid"-prootic suture (p-'p's) and sellar floor (sf) in a coronal section; B - the

1127 suture between the left and right supraoccipital, and the right supraoccipital and prootic in a horizontal

1128 section; C - a more ventral view of the prootic-supraoccipital and the flocular complex fossa (fcf) in a

1129 horizontal section; D - the prootic-opisthotic suture in a horizontal section; E - a sagittal section of the

1130 braincase showing the facial foramen (ff) ; F - a more medial sagittal section showing the prootic fossa

(prof) and the cerebral branch of the internal carotid (cbic) on the "parasphenoid"; G - horizontal section showing the sutures between the "parasphenoid", "basisphenoid", basioccipital and exoccipital; H - median sagittal view of the occiput showing the relationship of the tabular, supraoccipital, parietal and interparietal, notice the interparietal foramen (iparf); I - slightly more laterally offset sagittal section showing the interparietal canal (iparc) and the relationship of the supraoccipital, interparietal and parietal.

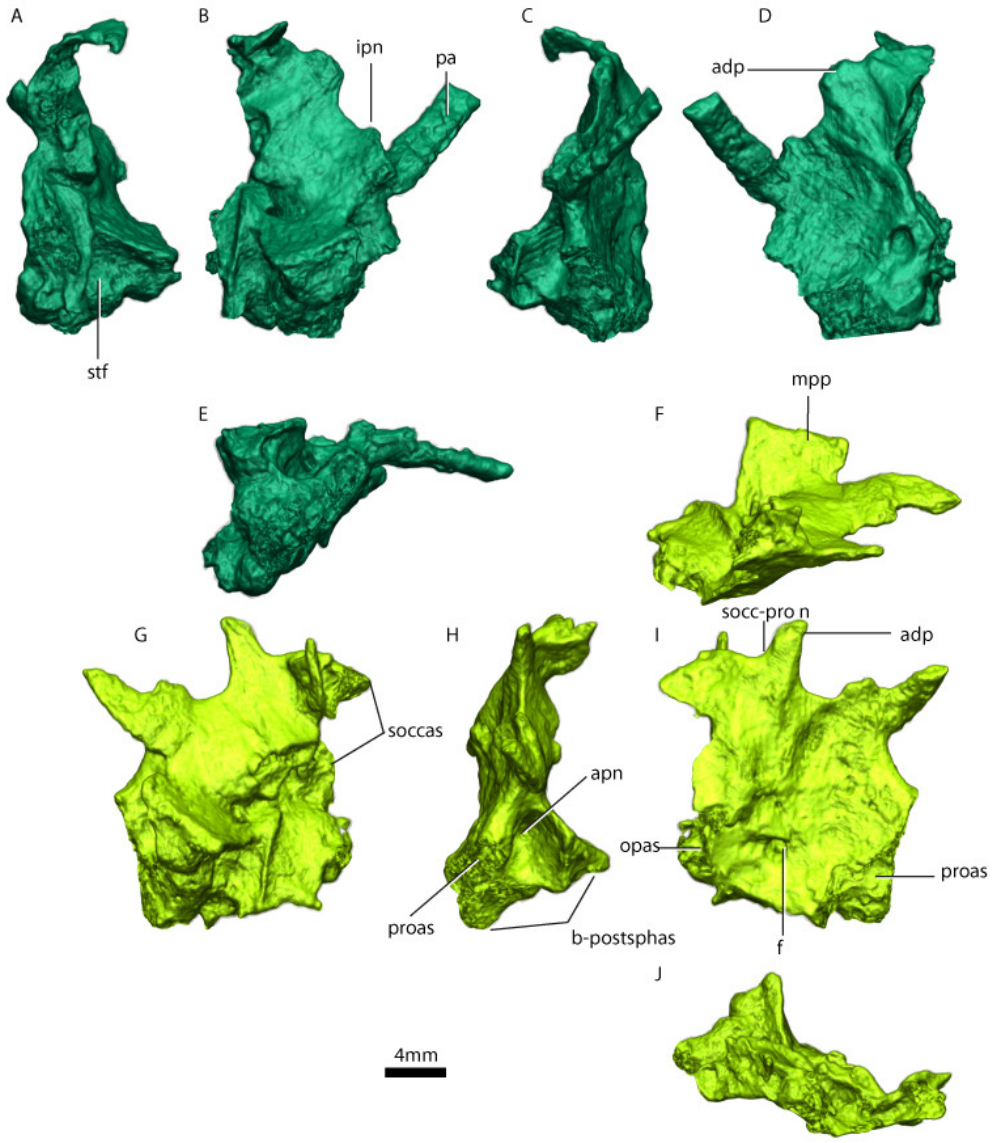

1138

1139

1140 Figure 5 – Left prootic in posterior (A), medial (B), anterior (C), lateral (D) and ventral views. Right

1141 prootic in dorsal (F), medial (G), anterior (H), lateral (I) and ventral (J) views. Abbreviations: adp –

1142 anterodorsal process, apn – anterior prootic notch, bpostspheas – basipostsphenoid articular surface, ff

1143 – facial foramen, ipn – interprocess notch, mpp – medial prootic process, opas – opisthotic articular

1144 surface, pa – pila antotica, proas – prootic articular surface, soccaf – supraoccipital articular facet, socc-

1145 pro n – supraoccipital-prootic notch.

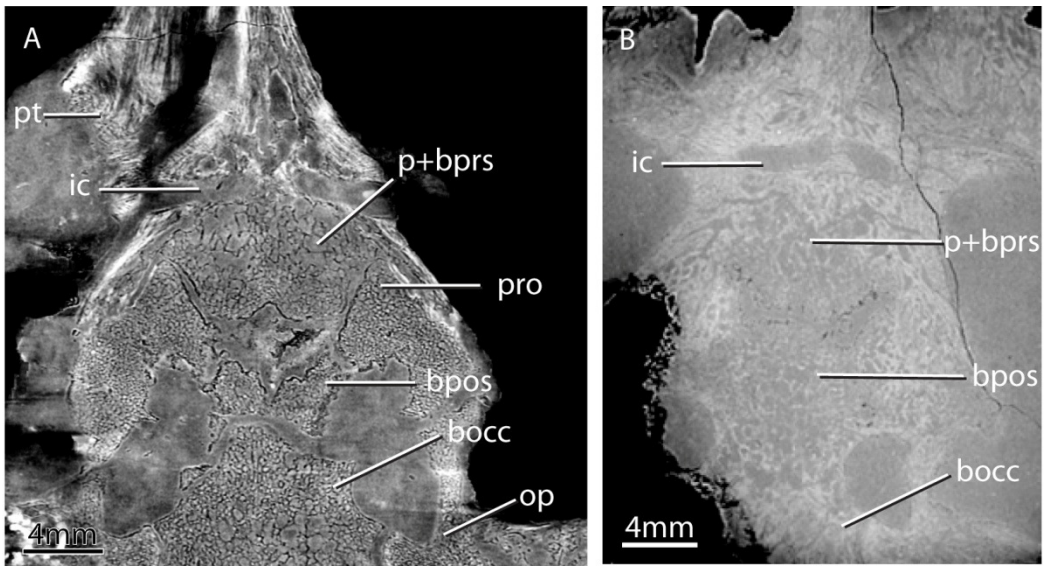

1146

1147 Figure 6 – Horizontal virtual sections of the skull of various gorgonopsian basicrania at different

1148 ontogenetic stages. Notice, for example, the wide separation between the basipostsphenoid and the

1149 parasphenoid-basipresphenoid complex in GPIT/RE/7124 (A) versus the condition in GPIT/RE/7119 (B).

1150 Abbreviations: bocc – basioccipital, bpos – basipostsphenoid , ic – internal carotids, op – opisthotic,

1151 p+bprs – parasphenoid-basipresphenoid, pro – prootic, pt – pterygoid.

1152

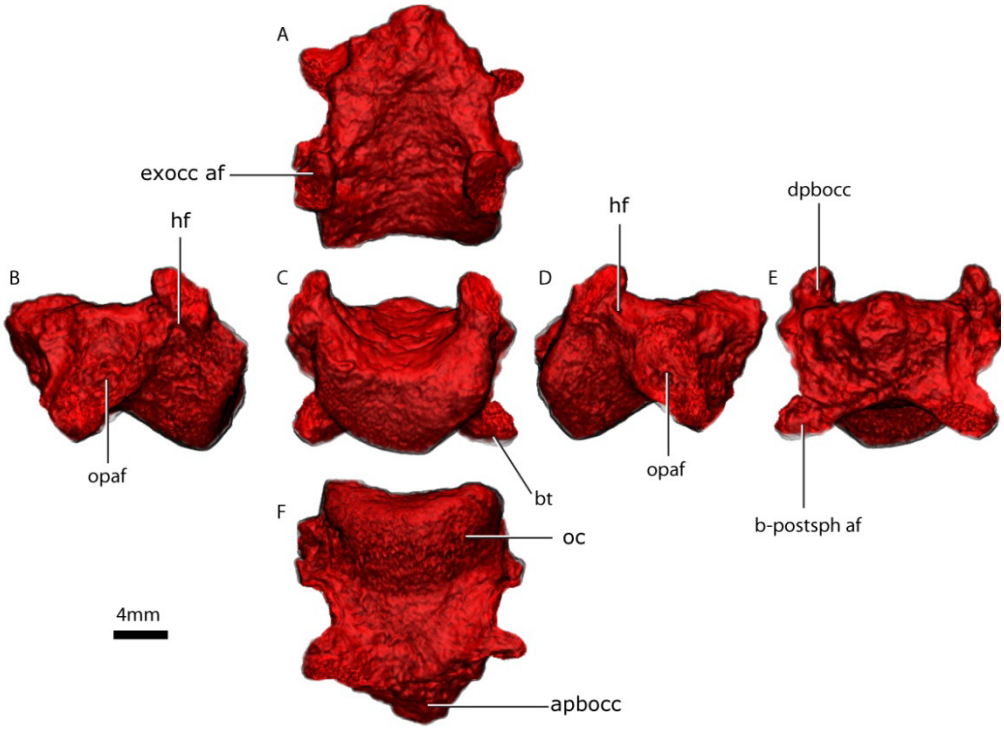

1153

1154

1155 Figure 7 – Basioccipital in ventral (A), lateral left (B), posterior (C) lateral right (D), anterior (E), and

1156 dorsal (F) views. Abbreviations: apbocc – anterior process of the basioccipital, bpostsph af –

1157 basipostsphenoid articular facet, bt – basal tubera, exocc af - exoccipital articular facet, hf – hypoglossal

1158 foramen, oc – occipital condyle, opaf – opisthotic articular facet.

1159

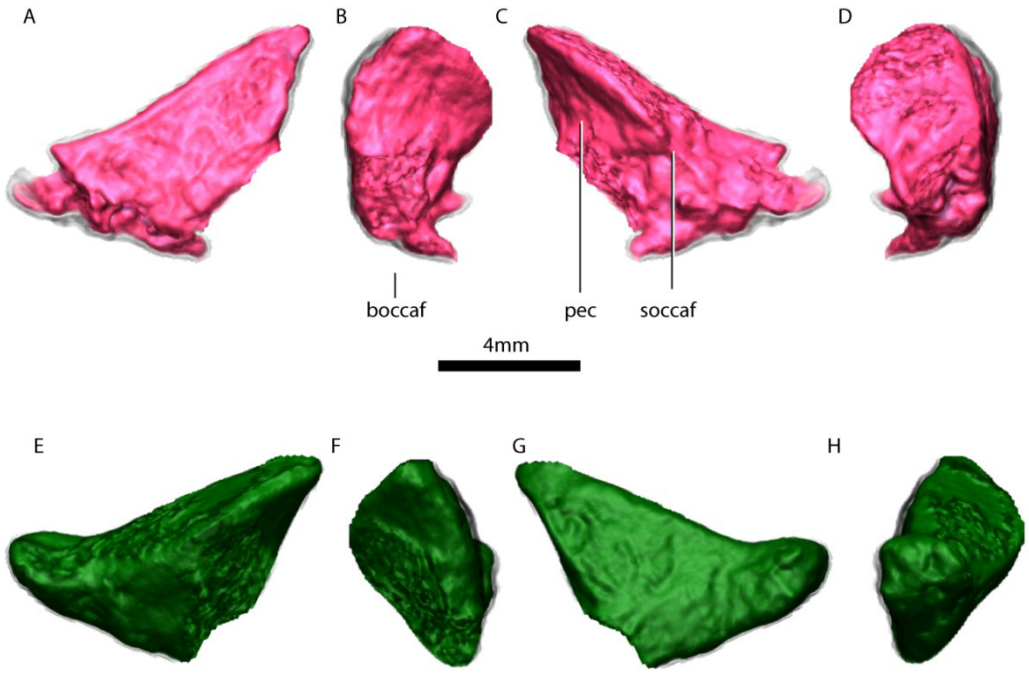

1160

1161

1162 Figure 8 – Right exoccipital in posterior (A), medial (B), anterior (C), lateral views. Left exoccipital in

1163 anterior (E), medial (F), posterior (G), lateral (H) views. Abbreviations: boccaf – basioccipital articular

1164 facet, pec – pyramidal exoccipital crest, soccaf – supraoccipital articular facet.

1165

1166

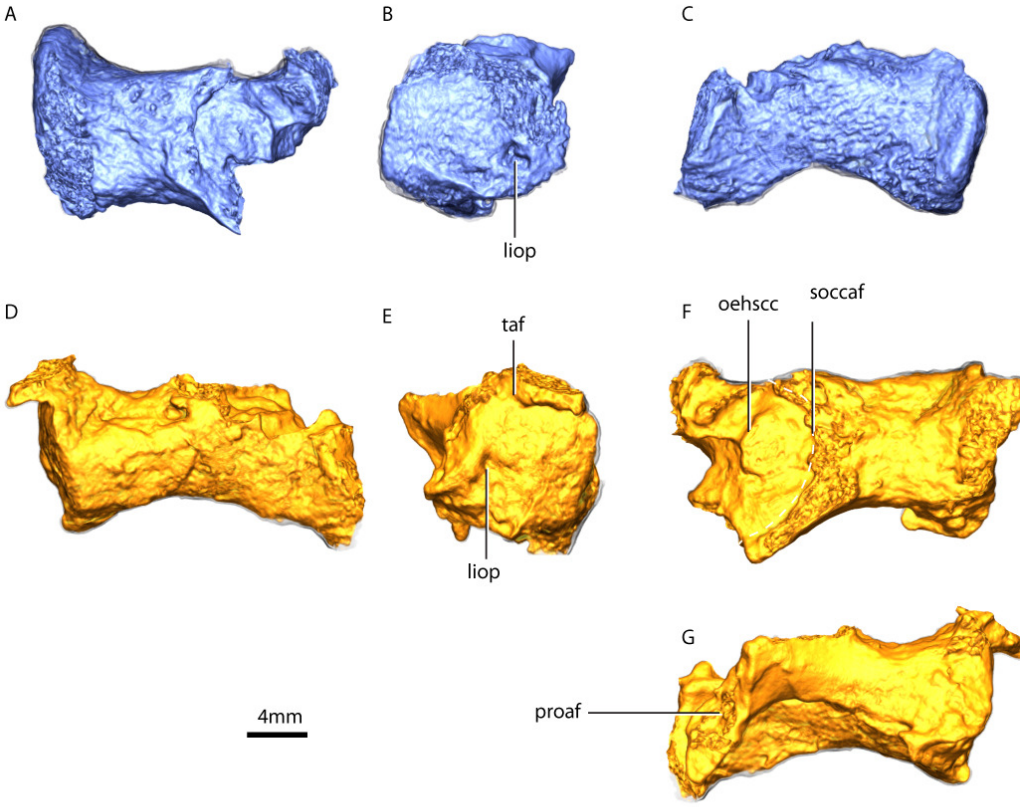

1167

1168

1169 Figure 9 – Right opisthotic in dorsal (A), lateral (B) and posterior (C) views. Left opisthotic in posterior

1170 (D), lateral (E), dorsal (F) and anterior (G) views. Abbreviations: liop – lateral incisure of the opisthotic,

1171 oehscc – osseous enclosure of the horizontal semicircular canal, proaf – prootic articular facet, soccaf –

1172 supraoccipital articular facet, taf – tabular articular facet.

1173

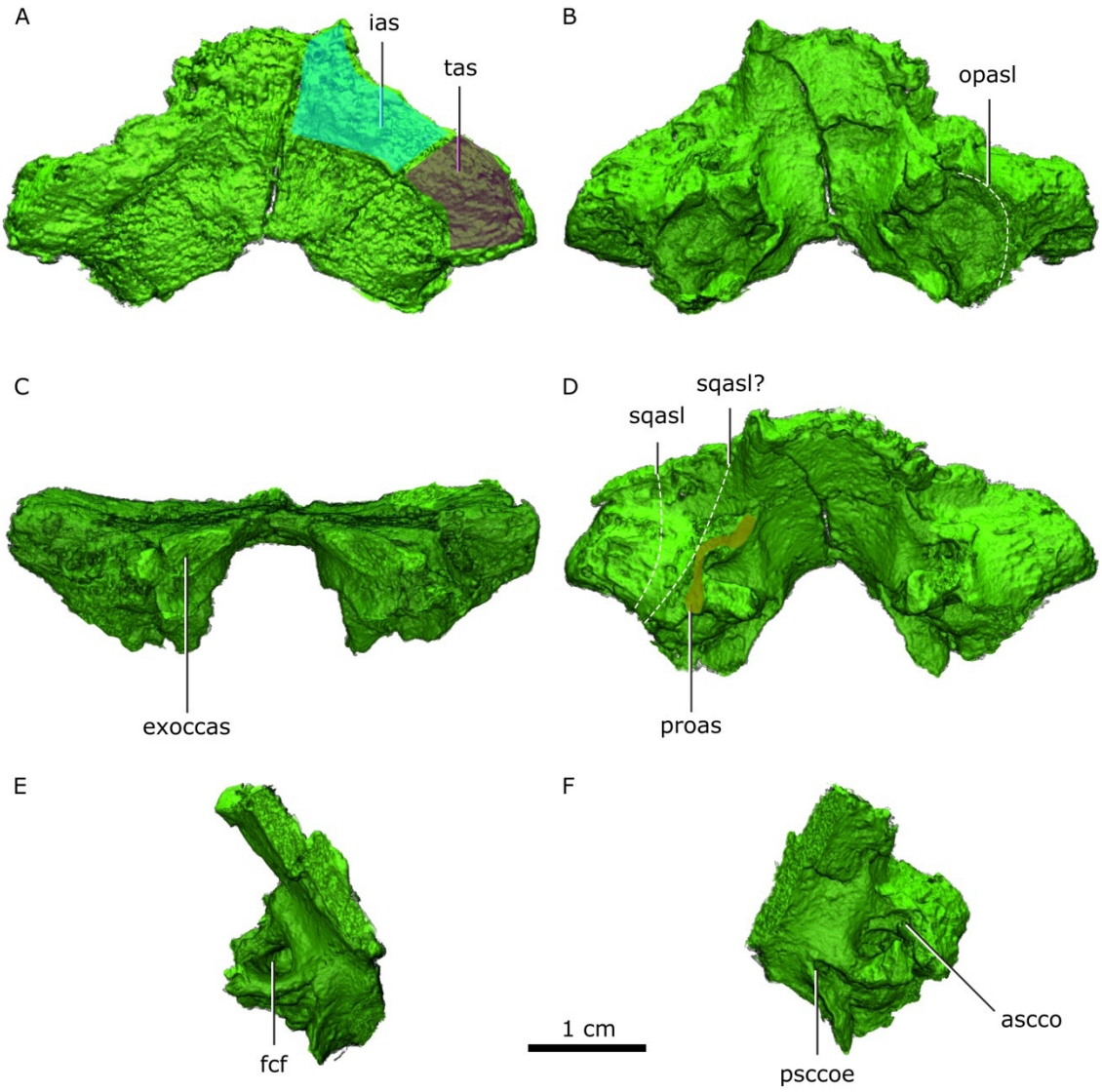

1174

1175

1176 Figure 10 – Supraoccipital in dorsal (A), ventral (B) posterior (C) and anteroventral (D) views. Right half

1177 of the supraoccipital in medial (E) view. Left half of the supraoccipital in medioventral (F) view.

1178 Abbreviations: asccoe – anterior semicircular canal osseous enclosure, exoccas – exoccipital articular

1179 surface, opasl – opisthotic articular surface limit, psccoe – posterior semicircular canal osseous

1180 enclosure, squas – squamosal articular surface limit as with the preserved portion of the squamosal and

1181 possible articular limit if the squamosal was entirely preserved, taf – tabular articular facet.

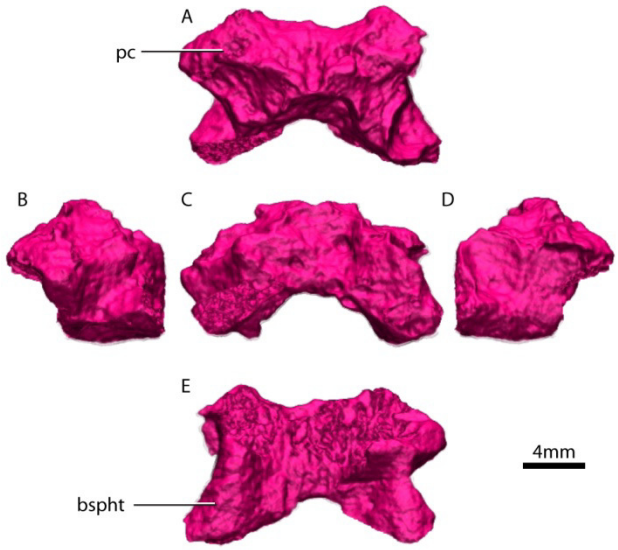

1182

1183 Figure 11 – Basipostsphenoid in dorsal (A), lateral left (B), posterior (C), lateral right (D), ventral (E)

1184 views. Abbreviations: bspht – basisphenoidal tubera, pc – parabolic crest.

1185

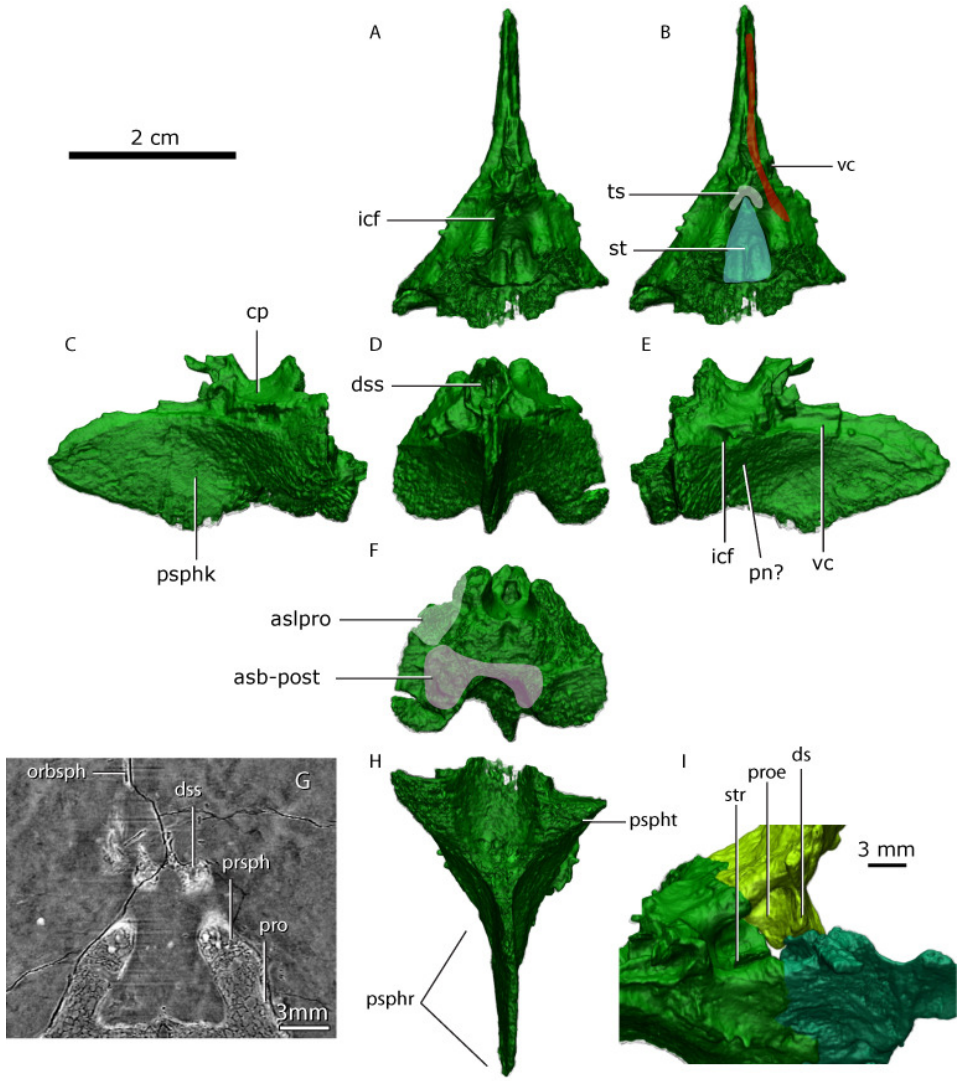

Figure 12 - Co-ossified parasphenoid and basipresphenoid in dorsal (A, B), lateral left (C), anterior (D), lateral right (E), posterior (F), ventral (G) and anterodorsal view with the prootics in articulation. Abbreviations: alspro – articular surface for the prootic, asbpost – articular surface for the basipostsphenoid , cp – clinoid process, ds – dorsum sella, dss – dome-shaped structure, icf – internal carotid foramina, pn – palatine nerve, proe – prootic embayment, psphk – parasphenoid keel, psphr – parasphenoidal rostrum, pspht – parasphenoidal tubera, st – sella turcica, str – sella turcica ridge, ts – tuberculum sella, vc – vidian canal.

1196

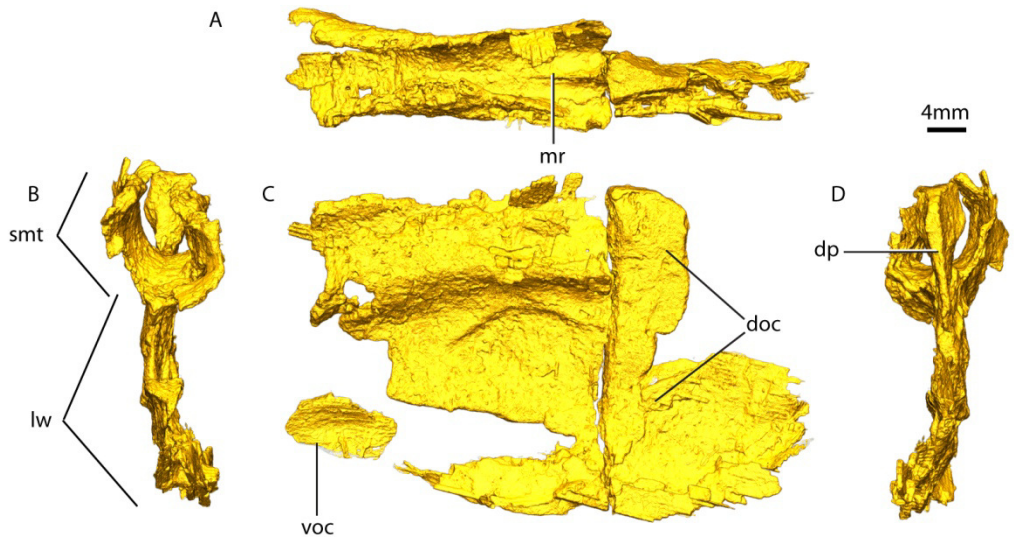

1198

1199 Figure 13 – Orbitosphenoid in dorsal (A), posterior (B), lateral (C) and anterior (D) views. Abbreviations:

1200 doc – dorsal ossification center, dp – dorsal process, lw – lateral wall, mr – median ridge, smt – semi-

1201 tubular region of the orbitosphenoid, voc – ventral ossification center.

1202

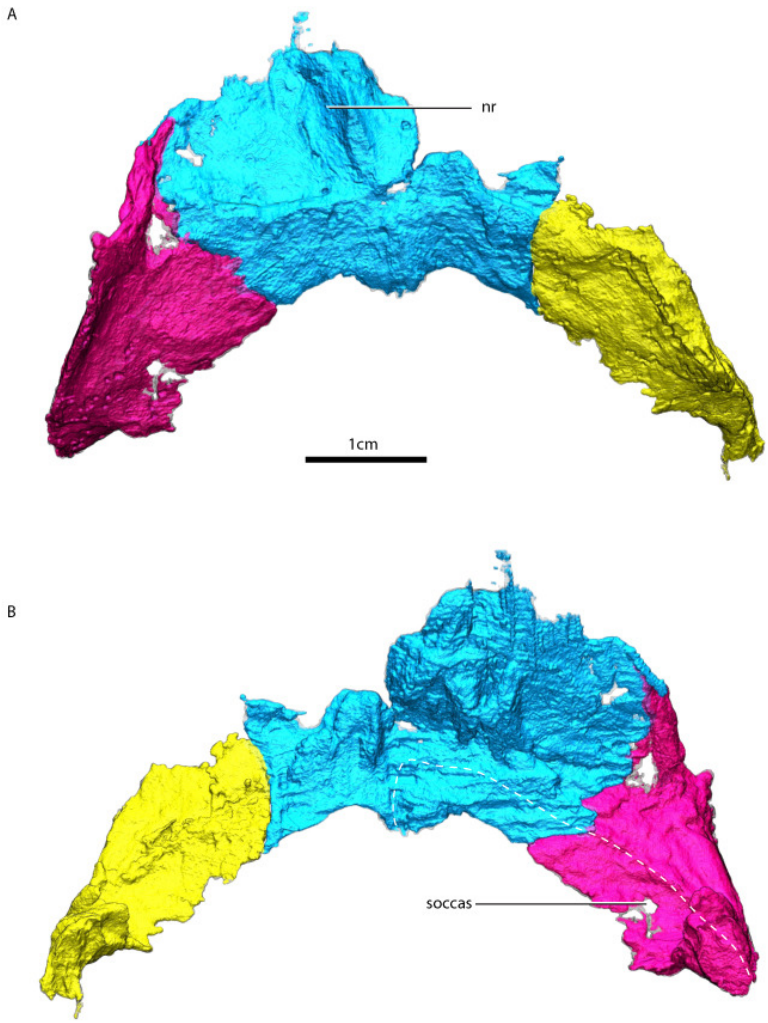

Fig 14 – Left and right tabulars and the interparietal in posterior (A) and anterior (B) views.

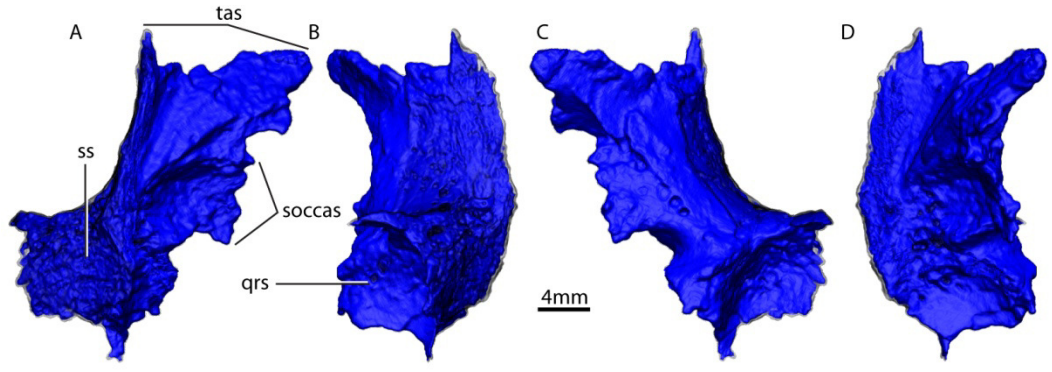

Figure 15 – Left squamosal in posterior (A), lateral (B), anterior (C) and medial (D) view. Abbreviations: qrs, quadrate recess of the squamosal, soccaf – supraoccipital articular facet, ss – squamosal sulcus, taf – tabular articular facet.

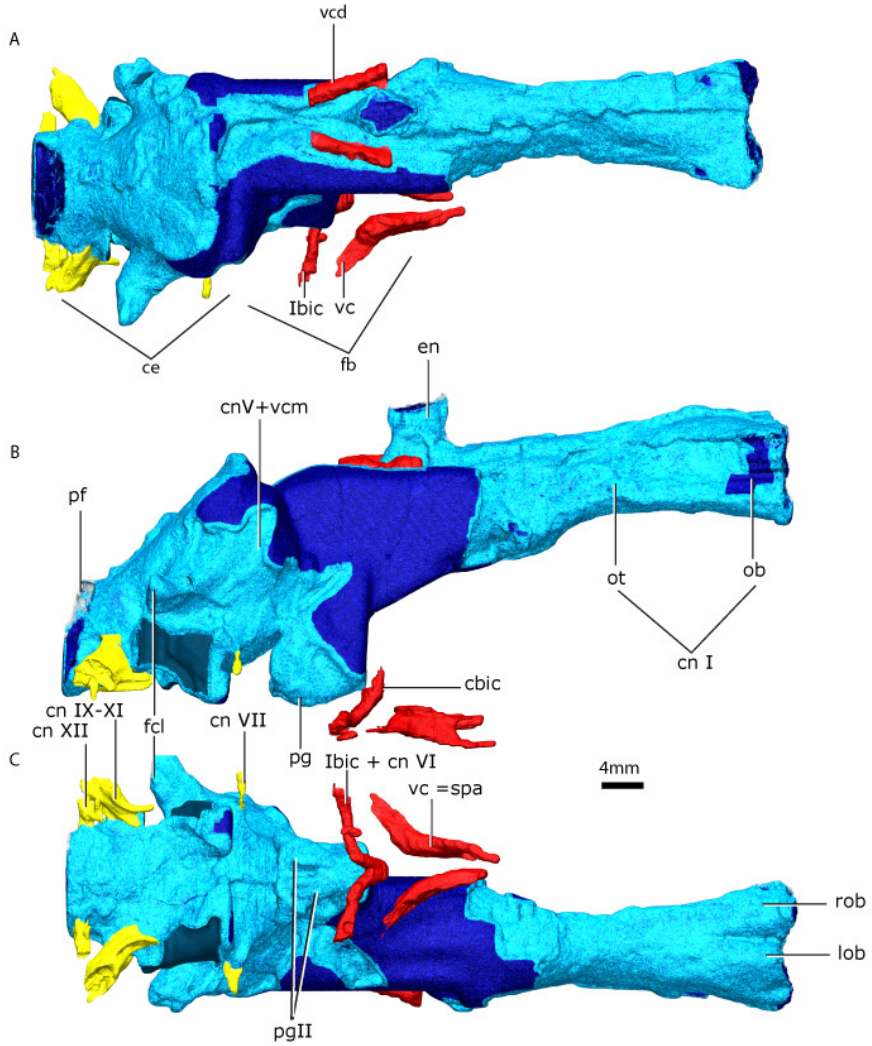

Figure 16 – Brain endocast in dorsal (A), lateral (B), ventral (C) views. Parts in light blue indicate direct contact with surrounding bones, unlike parts in darker blue. Abbreviations: ce – cerebellum, cnV+vcm - trigeminal nerve and vena capitis medialis, cnVI – abducens nerve, en – epiphyseal nerve, cnVII - facial nerve; cnIX-XI – glossopharyngeal and vagoaccessory nerves; cnXII - hypoglossal nerve, fb – forebrain, fcl

– floccular complex lobes, ibic – internal branch of the internal carotid, lob – left olfactory bulb, ob – olfactory bulb, ot – olfactory tract, pg – pituitary gland, pgll – pituitary gland lateral lobes, pf – pontine flexure, rob – right olfactory bulb, vc=spa – vidian canal where the sphenopalatine artery passes, vcd – vena capitis dorsalis.

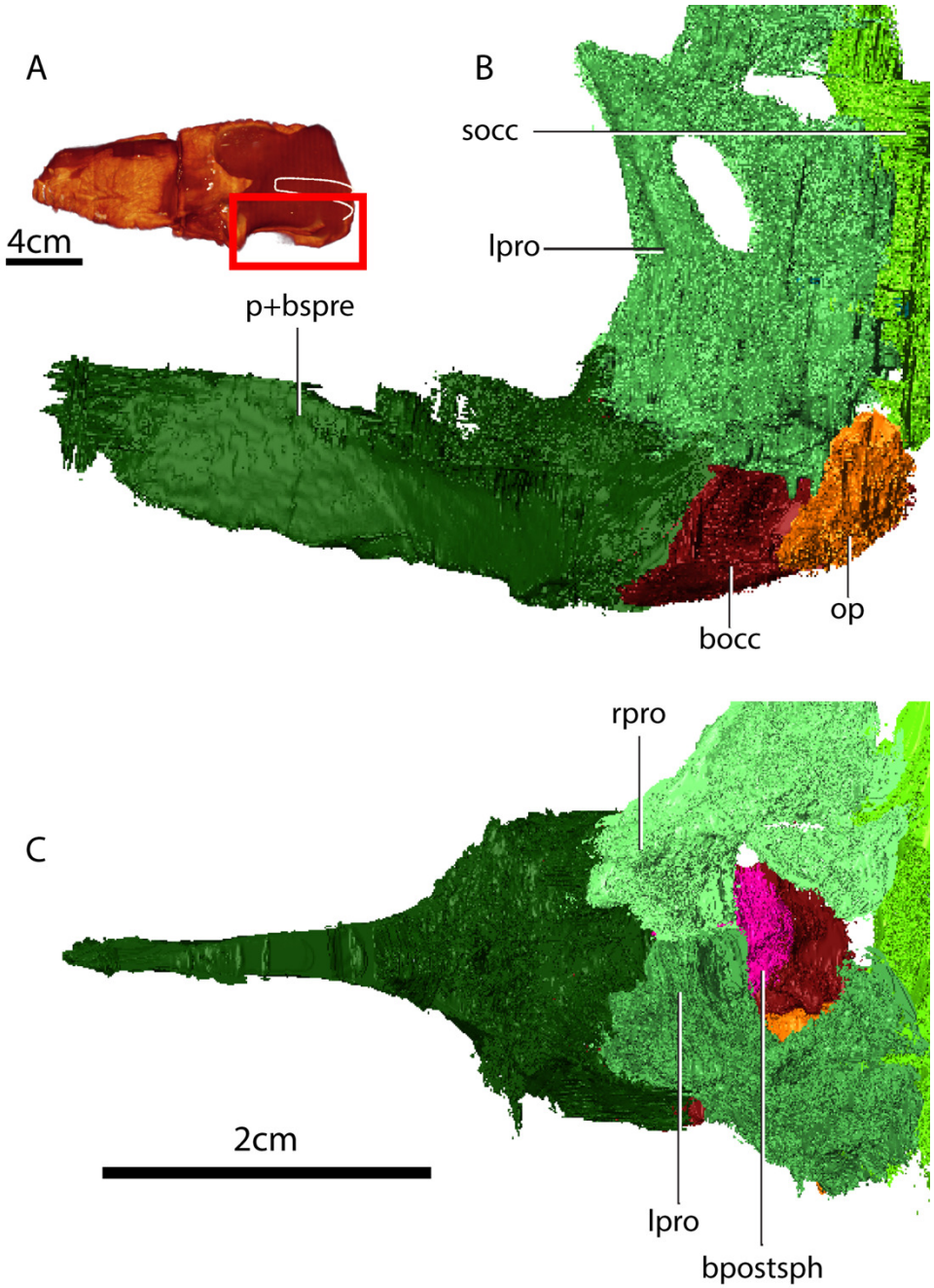

Figure 17 - GPIT/RE/7119 cranium in lateral view (A). Segmented portions of the basicranium in (B) lateral view, (C) dorsal view. Due to extensive co-ossification the more dorsal portions of the occiput the bones are impossible to extricate from each other in the tomographs. Abbreviations: p+bspre – parasphenoid and basipresphenoid, rpro – right prootic, lpro – left prootic, bpostsph – basipostsphenoid, bocc – basioccipital. op – opisthotic, socc – supraoccipital.

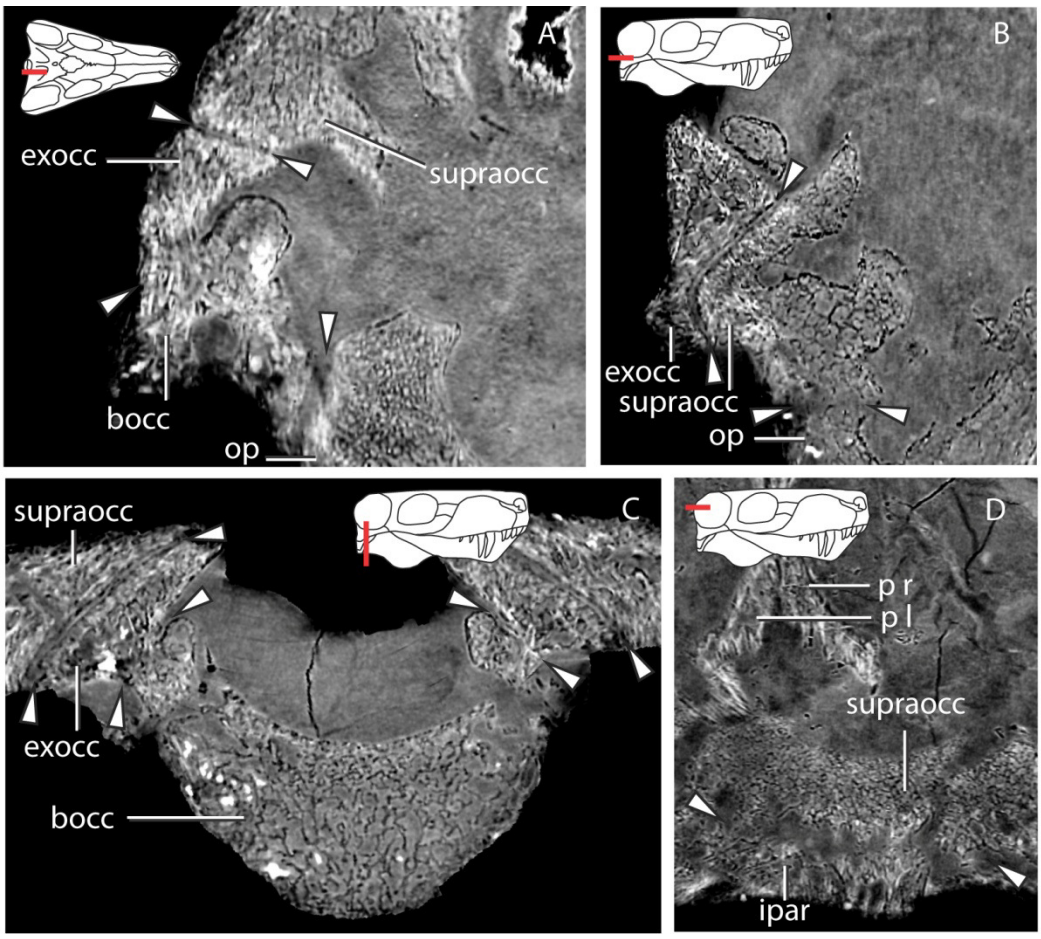

Figure 18 – Contentious issues concerning the gorgonopsian occiput clarified by GPIT/RE7124. A, B, C show that the exoccipital does not contact the opisthotic. A, sagittal section through the right exoccipital; B, horizontal section through the right exoccipital, supraoccipital and opisthotic; coronal section through the basioccipital and the two exoccipitals. D, shows the suture and overlap between the supraoccipital and interparietal. Abbreviations: bocc – basioccipital, exocc – exoccipital, ipar –

1232 interparietal, op – opisthotic, p l – left parietal, p r – right parietal, supraocc –supraoccipital. Arrows

1233 show the locations of the sutures between bones.

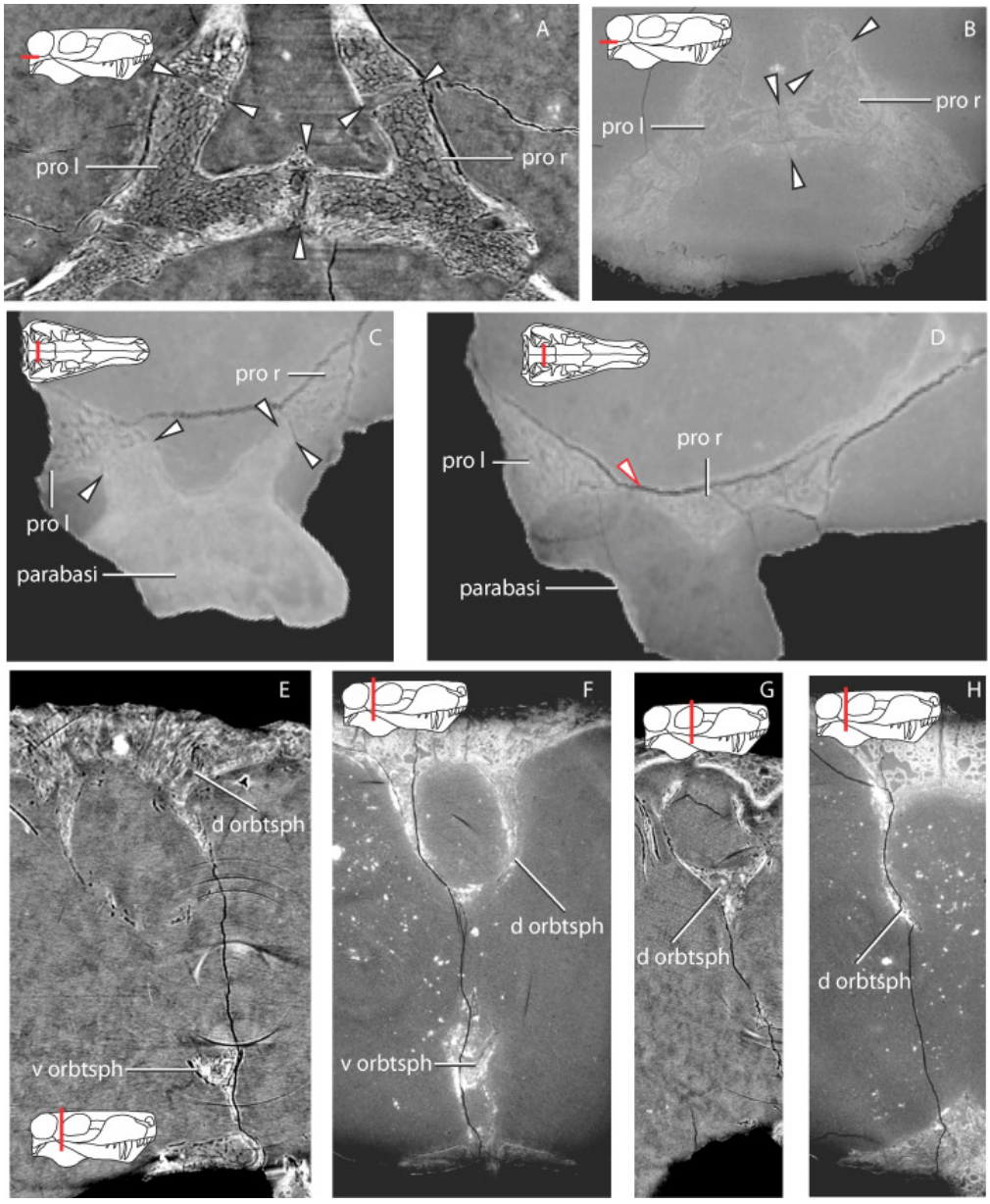

1234

1235 Figure 19 – Comparisons of virtual cross sections through the basicranium. A, GPIT/RE/7124 horizontal

1236 section through the prootics; B, GPIT/RE/7119 horizontal section through the prootics at a similar

1237 location of A; C, coronal section through the prootics and parabasisphenoid of the therocephalian

1238 GPIT/RE/7139; D, more posterior coronal section through the prootics (the parabasisphenoid is not

1239 preserved in this region, except for a small splinter of bone); the ventral ossification center of the

orbitosphenoid and the dorsal ossification center in GPIT/RE/7124 and GPIT/RE/7119 in E and F, respectively; and in a more anterior coronal section only the dorsal ossification center of the orbitosphenoid in GPIT/RE/7124 and GPIT/RE/7119 in G and H, respectively. Black arrows indicate the sutures between the bones and the red arrow the contact between the two prootics.

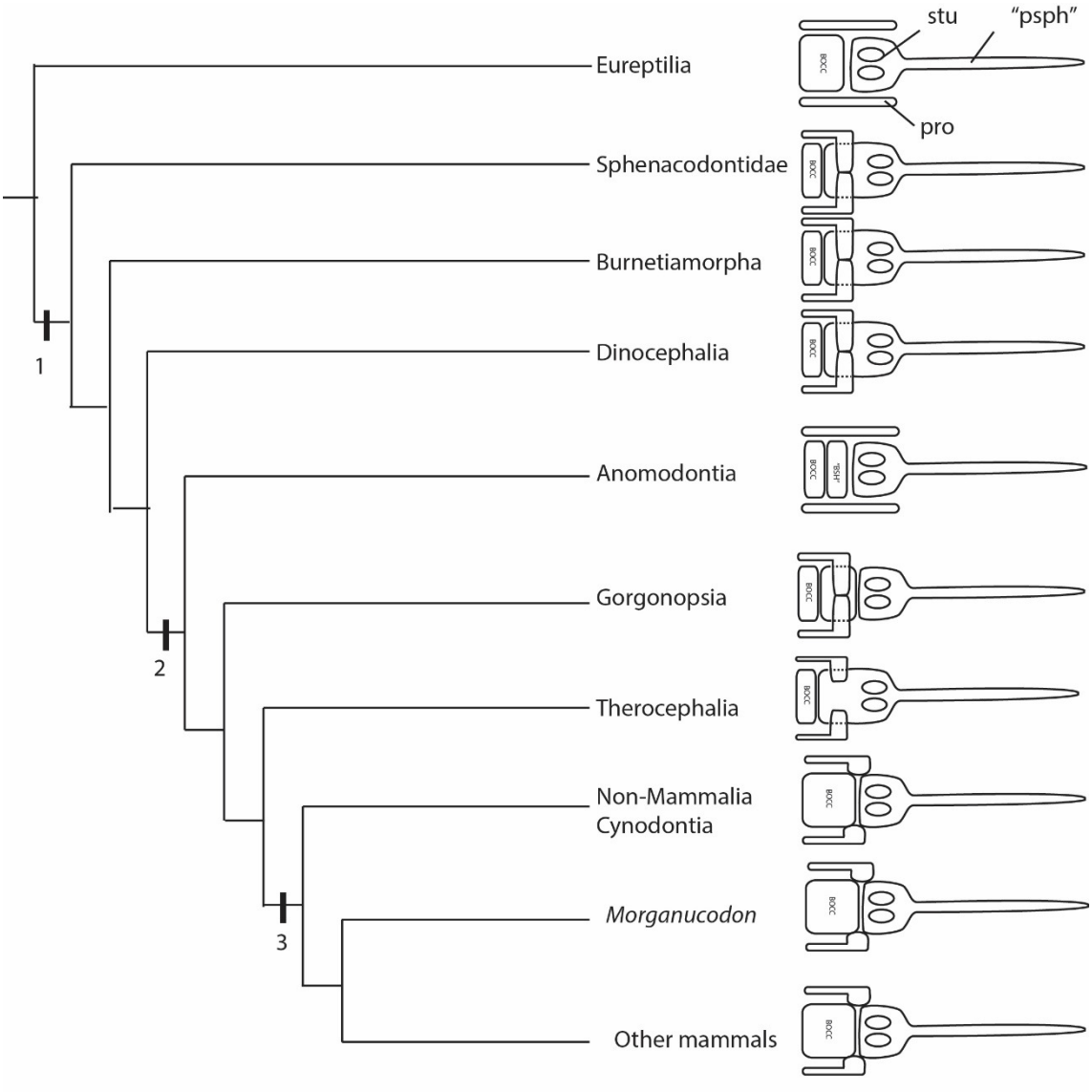

Figure 20 – Major anatomical and developmental transformations of the parasphenoid, basisphenoid, prootic, basioccipital complex in synapsids: 1 - Synapsida: Morphology: formation of the medial prootic process, prootics meet medially; Development: invasion of the otic capsule cartilage onto the basal plate

region. 2 - Theriodontia: Morphology: reorganization of the prootic and parabasisphenoid complex; basipostsphenoid becomes a separate ossification; Development: shift of the neural crest - mesoderm boundary (or prechordal-chordal skull boundary). 3 - Cynodontia: Morphology: petrosal (opishtotic + prootic) contacts parabasisphenoid complex Development: possible supression of the mesoderm-derived posterior portion of the basisphenoid due to induction of the otic capsule cartilage.

Abbreviations: bocc, basioccipital; “psph”, parasphenoid but here parasphenoid + basi-presphenoid; “bsh” basisphenoid but here basipostsphenoid; stu, sella turcica; pro, prootic.

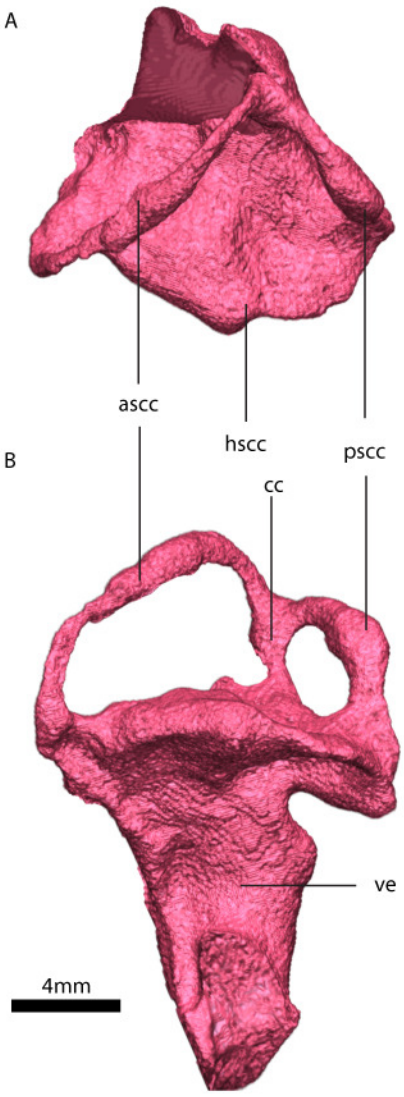

Figure 21 – Left osseous in dorsal (A) and lateral (B) views. Abbreviations: asccoe – anterior semicircular canal osseous enclusure, cc – crus communis, psccoe – posterior semicircular canal osseous enclusure, ve – vestibule.

1260

1261 Figure 22 – Head posture of GPIT/RE/7124 if the horizontal semicircular canal is aligned with earth

1262 plane.